

Reviews on innovations and applications in structural health monitoring for infrastructures

Hong-Nan Li^{*}, Ting-Hua Yi^a, Liang Ren^b, Dong-Sheng Li^c and Lin-Sheng Huo^d

Faculty of Infrastructure Engineering, Dalian University of Technology, Dalian 116023, China

(Received February 11, 2014, Revised March 10, 2014, Accepted March 19, 2014)

Abstract. The developments and implementations of the structural health monitoring (SHM) system for large infrastructures have been gradually recognized by researchers, engineers and administrative authorities in the last decades. This paper summarizes an updated review on innovations and applications in SHM for infrastructures carried out by researchers at Dalian University of Technology. Invented sensors and data acquisition system are firstly briefly described. And then, some proposed theories and methods including the sensing technology, sensor placement method, signal processing and data fusion, system identification and damage detection are discussed in details. Following those, the activities on the standardization of SHM and several case applications on specific types of structure are reviewed. Finally, existing problems and promising research efforts in the field of SHM are given.

Keywords: structural health monitoring; infrastructure; sensing technology; signal processing; system identification

1. Introduction

With the extensive utilization of key infrastructures, such as long-span bridges, large-scale space structures, and high-rise buildings, in various engineering applications, the need of accurate and robust structural health monitoring (SHM) techniques for them has been the major topic of many research efforts striving to enhance the safety and reliability, while reduce the operation and maintenance costs of the infrastructures (Wenzel 2009). Recent advances on sensing, communication, and storage technologies have also enabled the use of broad-scale SHM system to the infrastructures. The so-called SHM, formally defined by Housner *et al.* in the late 20th century, refers to the use of in-situ, continuous or regular measurement and analyses of key structural and environmental parameters under operating conditions, for the purpose of warning impending abnormal states or accidents at an early stage to avoid casualties as well as giving maintenance and rehabilitation advice (Housner *et al.* 1997). In general, a typical SHM system includes three major components: a sensor system, a data processing system (including the data acquisition,

*Corresponding author, Professor, E-mail: hnli@dlut.edu.cn

^a Professor, E-mail: yth@dlut.edu.cn

^b Associate Professor, E-mail: renliang@dlut.edu.cn

^c Associate Professor, E-mail: dqli@dlut.edu.cn

^d Associate Professor, E-mail: lshuo@dlut.edu.cn

transmission and storage), and a health evaluation system (including the diagnostic algorithm and information management) (Mufti 2002). The SHM systems are generally envisaged to: validating the modification to an existing structure; assessing the safety and performance of structures affected by external works; tracking a long term movement or degradation of materials in critical structures; providing a feedback loop to design; estimating the fatigue life; checking the novel systems of construction and new structural forms; evaluating the post-earthquake structural integrity; enhancing the effectiveness of resources as construction declines and maintenance needs increase; catering for the move towards performance-based design philosophy; etc. (Brownjohn 2007).

Over the last decade, the developments in this most rapidly increasing research field have attracted the special interests to the scientists and engineers. Successful implementations of long-term SHM systems to infrastructures have been widely reported in the literature (Zhou and Yi 2013a, Zhou and Yi 2013b). Typical examples are mostly on long-span bridges, such as the Confederation Bridge in Canada (Cheung *et al.* 1997), the A14 Huntingdon Railway Viaduct in United Kingdom (Cullington *et al.* 1999), the Akashi Kaikyo Bridge in Japan (Kashima *et al.* 2001), the Tuas Second Link between Singapore and Malaysia (Brownjohn and Moyo 2001), the Great Belt Bridge in Demark (Henrik and Denmark 2002), the Saint-Jean Bridge in France (Magne *et al.* 2003), the Tsing Ma Bridge in Hong Kong of China (Wong 2004), the Sunshine Skyway Bridge in United States (Schenewerk *et al.* 2006), the Europabrücke bridge in Austria (Wenzel 2009), the Sutong Bridge in mainland of China (Chen *et al.* 2010). Some other experiences in a number of real world applications of SHM were also widely reported. For example, the two high-rise buildings in United States (Kijewski-Correa *et al.* 2006), the new Circle Line Stage 3 subway in Singapore (Mohamad *et al.* 2007), the Marco Polo tension leg platform in United States (Dijk and Boom 2007), the Canton Tower in mainland of China (Ni *et al.* 2009), the San Siro Meazza stadium in Italy (Cigada *et al.* 2010). Far too many applications exist to mention them all in this paper. With the widespread implementation of SHM technology, its real-time and long-term role is gradually revealed. For instance, the monitored vibration amplitude in the Akashi Kaikyo Bridge was found only about one-third of the calculated value using the wind-resistant design standard. Through the gust response analysis and field monitoring data of natural winds, it was found that the actual value for spatial correlation in the natural wind was lower, in the low frequency region, than the spatial correlation assumed in the wind resistant design standard (Kashima *et al.* 2001). This provides a good basis for the revision of wind resistant design standard. Peeters and Roeck (2001) conducted a study devoted to monitoring the effect of changing environmental conditions on structural vibration properties on the Z24 Bridge in Switzerland. It was observed that the first four vibration frequencies varied by 14% ~ 18% during the 10 months. Without a doubt, the SHM system can offer valuable information in evaluating structural durability, reliability and integrity, and in ensuring optimal maintenance planning and safe infrastructure operations. Directions in the SHM are being identified as advanced sensing (smart, bio-inspired, nanometer, wireless, and remote sensing, etc.); massive data management and storage; efficient data mining, fusion, diagnostic and identification methods, and presentation of timely and reliable information to infrastructure managers for the decision making on maintenance (Ko and Ni 2005).

This paper demonstrates some innovative work carried out by the “research center for structural health monitoring and control (RCSHMC)” in Dalian University of Technology, China. The content of the paper is organized as follows: Section 2 gives a brief overview of the invented sensors and data acquisition system after the introduction. Section 3 presents the proposed theories

and methods in the SHM. Section 4 describes the activities on standardization of SHM. Section 5 shows some typical infrastructures applications. Finally, the paper is concluded in Section 6.

2. Novel sensors and data acquisition system

Conventional sensors and corresponding data acquisition system are usually infeasible to apply to large infrastructures for long-term monitoring, which make the advanced sensor and acquisition system become one of the major focuses of the SHM research (Shang *et al.* 2012, Bai *et al.* 2012). Particular examples developed in the RCSHMC are novel fiber optic sensors (FOS), global positioning system (GPS), piezoelectric transducers (PZT) and data synchronous acquisition system (DSAS).

2.1 Fiber Bragg grating sensor

(1) FBG strain sensor

The schematic diagram of a FBG strain sensor is presented in Fig. 1, which consists of a fiber Bragg grating, two gripper tubes and two mounting supports (Ren *et al.* 2009). The fiber in both sides of a FBG is packaged with the epoxy resin in two gripper tubes, which are installed on the mounting supports by the adhesive or solder. Since the FBG area is not in contact with the epoxy resin, the FBG strain sensor eliminates multi-peaks of reflective light from the FBG induced by the non-uniform bonding distribution of epoxy resin. When the thickness of the glue is less than the diameter of an optical fiber, the stress transferring loss between the epoxy resin and fiber can be neglected, as it has been discussed in detail, and the deformation of gripper tube and FBG are written by

$$\Delta L_s = \frac{P_s L_s}{E_s A_s}, \quad \Delta L_f = \frac{P_f L_f}{E_f A_f} \quad (1)$$

where E_s , E_f , A_s and A_f are the Young's modulus and sectional area of gripper tube and fiber, the distance between two mounting supports and the length of fiber are L and L_f , and P_s and P_f are the internal tension forces in the fiber and the gripper tubes, respectively.

Since values of tension forces are constant throughout the sensor structure, P_s equals to P_f . Therefore, the strain ratio between the gripper tube and fiber can be expressed as follows

$$\frac{\varepsilon_s}{\varepsilon_f} = \frac{\Delta L_s / L_s}{\Delta L_f / L_f} = \frac{E_f A_f}{E_s A_s} \quad (2)$$

Table 1 presents the mechanical properties of the FBG strain sensor. The strain ratio is obtained by substituting the parameter values into Eq. (2) as

$$\frac{\varepsilon_s}{\varepsilon_f} = 0.0084 \quad (3)$$

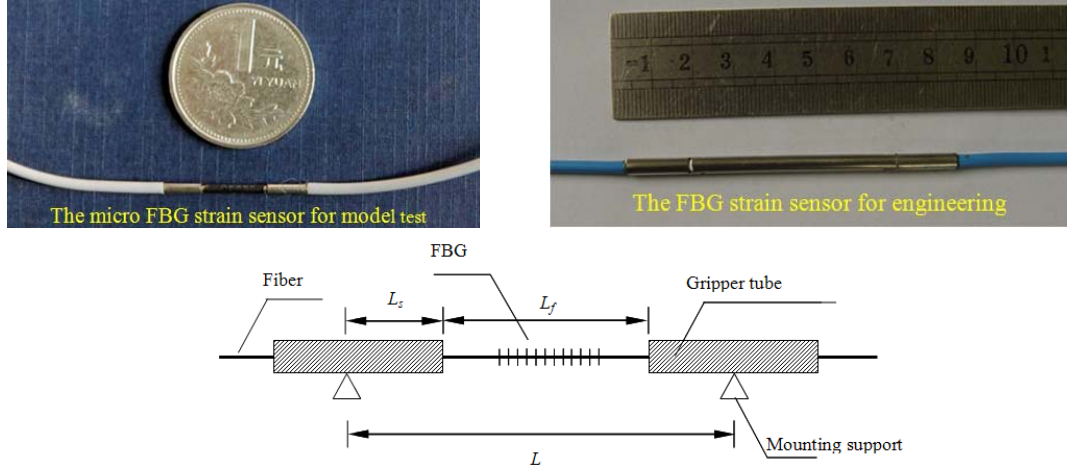


Fig. 1 Pictures and schematic diagram of FBG strain sensor packaged by two gripper tubes

Table 1 Mechanical properties of the optical fiber

Component	Young's modulus[Pa]	Diameter[mm]
Fiber core (E_f)	72×10^9	0.125
Gripper tube (E_s)	210×10^9	0.8

It is drawn from Eq. (3) that the strain of gripper tube can be neglected in contrast with the strain of fiber in the above sensor construction. The fiber between two gripper tubes bears nearly the whole deformation between two mounting supports. For a FBG with the central wavelength of 1550 nm, the relation between the shift of the central wavelength of FBG and strain of sensor can be written by

$$\varepsilon = \frac{L_f}{L} \varepsilon_f = \frac{L_f \Delta \lambda_{FBG}}{1.2L} \quad (4)$$

The strain sensitivity of sensor is determined by the ratio of distance between two mounting supports L and the length of fiber between two gripper tubes L_f , as shown in Eq. (4). For the case that L is bigger than L_f , the sensor has a mechanical structure of strain sensitivity amplification. A suitable strain sensitivity of FBG strain sensor can be obtained by adjusting the ratio between L_f and L .

To characterize the working performance of FBG strain sensor in the dissimilar host material with the different Young's modulus, a series of calibration tests of FBG strain sensor were conducted on the steel and plastic plates, of which the Young's modulus were 2.1×10^5 MPa and 3×10^3 MPa respectively. A FBG strain sensor and a strain gage were mounted directly on the plates within the cyanoacrylate adhesive. Then, the tensile tests in the steel and plastic plates were carried out in the material testing system. Experimental strain sensitivities of FBG strain sensor in the steel and plastic plates are $0.501 \mu\epsilon/\text{pm}$ and $0.487 \mu\epsilon/\text{pm}$, respectively, as shown in Fig. 2. The experimental values agree well with the calculated strain sensitivity of FBG sensor. In addition, the strain transferring loss in the plastic plate is very small and can be neglected. Results prove that the

FBG strain sensor works well on the host materials with the low Young’s modulus, such as plastic. Reliability is an important aspect of any sensor, especially in terms of long-term monitoring of civil structures, such as dams with 50 ~ 100 years of service life. In order to investigate the reliability of FBG strain sensor, a standard steel plate, on which the small scale FBG strain sensor were mounted by the epoxy, was used as a test structure with a continuous deformation loaded by a material test machine (MTS810) in the Fig. 3, which applied axial force from 0 to 10 kN at a constant frequency with 20 Hz. The maximum and minimum wavelength values of FBG strain sensor kept constant in the Fig. 4 during the fatigue test with 45,000 cycles. The minor shift of wavelength peak, which is only 40 pm, can be neglected for the thermal expansion of sample plate and the micro variation of force actuated by the MTS machine. The results demonstrate that the behavior of FBG strain sensors is steady and repeatable in the reliability test.

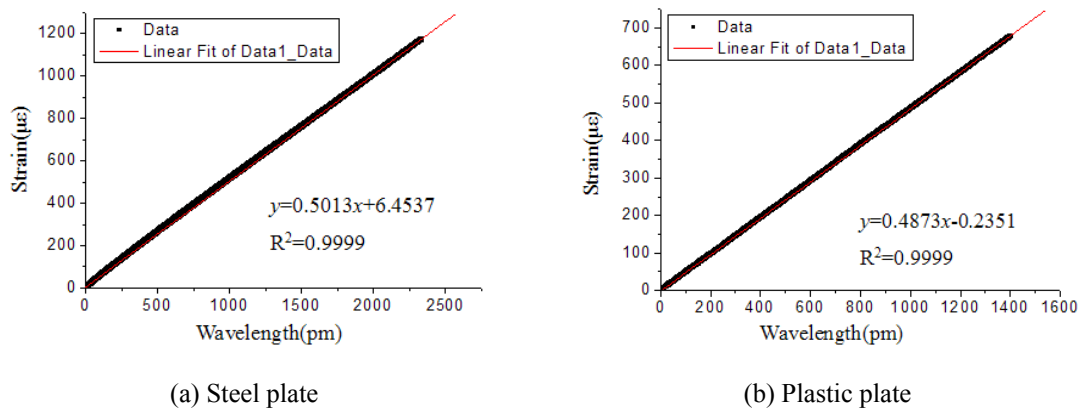


Fig. 2 Results of FBG strain sensor calibration tests

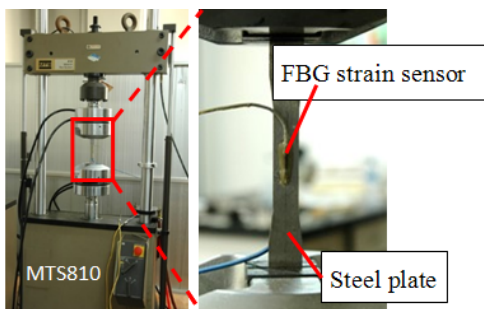


Fig. 3 Fatigue reliability test set-up of FBG strain sensor

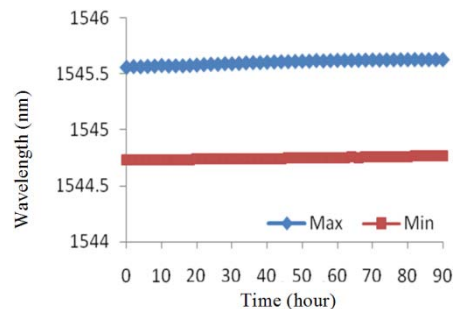
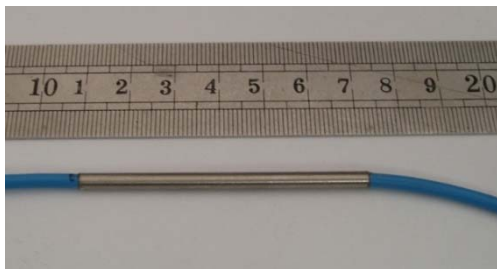


Fig. 4 Data of loading circles saved in first operating conditions

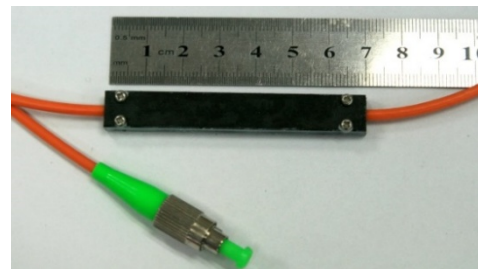
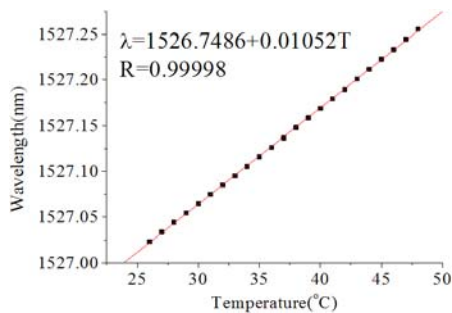
(2) FBG temperature sensor

It is known that the wavelength shift of reflected light is influenced by both strain and temperature. For a bare FBG without any packaging, the sensitivity from strain, which is about $1.2 \text{ pm}/\mu\epsilon$, is usually much higher than the temperature which is about $10.8 \text{ pm}/^\circ\text{C}$ at $\lambda_B = 1510\text{-}1590 \text{ nm}$. In the design of FBG temperature sensor, several novel techniques are presented available to eliminate the adverse effect of strain and remarkably improve the thermal sensitivity.

For the FBG temperature sensor to be attractive for practical application, the outer shape of sensor housing is of significance. Fig. 5 shows the examples of FBG temperature sensors with the enhanced and non-enhanced sensitivities which was packaged by a stainless steel tube and cube respectively. For the purpose of sensor calibration, the FBG sensor was totally immersed in the epoxy resin. By controlling the temperature of the epoxy resin, the Bragg wavelength changes of FBG temperature sensor accordingly are measured. Thus, the FBG temperature sensor can be calibrated by comparing with the measured temperature difference. The FBG temperature sensor shows a rapid slope of its $\lambda_B(T)$ characteristics in Fig. 5(a). The temperature sensitivity is $\partial\lambda_B/\partial T = 26.89 \text{ pm}/^\circ\text{C}$, and is approximately three times larger than the theoretical value of a bare fiber Bragg grating, which is typically $\partial\lambda_B/\partial T = 10.8 \text{ pm}/^\circ\text{C}$ at the wavelength range of $\lambda_B = 1510\text{-}1590 \text{ nm}$. Considering the wavelength accuracy of demodulation system is 1 pm , the measurement accuracy of tube-packaged FBG temperature sensor exceeds 0.1°C .



(a) FBG temperature sensor with enhanced sensitivity



(b) FBG temperature sensor with non-enhanced sensitivity

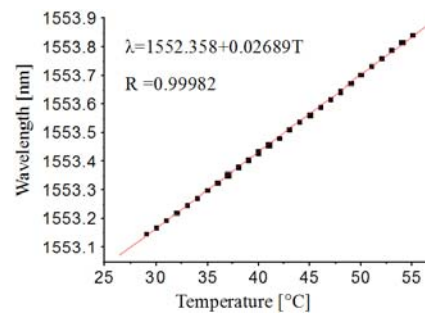


Fig. 5 Temperature sensing characteristics of FBG temperature sensors with non-enhanced and enhanced sensitivities

2.2 Piezoelectric transducer

In recent years, the piezoelectric sensors manufactured by the Lead Zirconate Titanates (PZT), have been widely applied to the SHM due to their characters of electromechanical coupling, simple structure, low cost, good reliability and widely frequency response range.

For the piezoelectric effect, the PZT sensors can be used both as sensors which can receive the static or dynamic strain from host structures, and actuators to excite vibration and elastic wave for the SHM system. The PZT sensors can be adhered or embedded in structures to monitor the status of civil infrastructures. Song *et al.* (2008) explored a type of embedded PZT sensors called “smart aggregate”. Similar to the smart aggregate, Zhao (2008) invented a type of embedded cement-based PZT sensor as shown in Fig. 6. The explored cement-based PZT sensor is composed by the PZT patch, waterproof layer by the epoxy resin, electric wires and cement protective layer as shown in Fig. 7. The PZT patch is first welded with electric wires on both electrode surfaces, and then is covered by the epoxy resin to keep off water as shown in Fig. 8. At last, the PZT patch is embedded by the cement with the dimension of aggregate. This type of PZT sensors has two advantages. Firstly, the dimension of sensors is similar to the aggregate, which has no influence on the mechanical performance of host structures. Besides, the property of cement is analogous to concrete, and the propagation of elastic wave will not be changed from host structures to the PZT patch. Zhao (2008) conducted the calibration experiments to test the mechanical performance of embedded PZT sensors. The schematic diagram of test is shown in Fig. 9. The loading and output curves from the sine wave, sweep wave and square wave are shown in Fig. 10, which show the good responsibility of sensors.



Fig. 6 Embedded cement based PZT sensor (Zhao 2008)

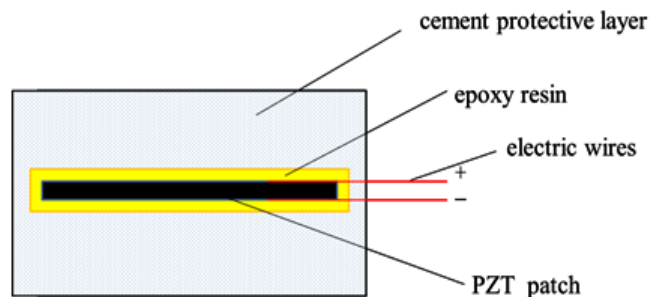


Fig. 7 The illustrate of the embedded PZT sensors (Zhao 2008)



Fig. 8 the waterproof layer by epoxy resin (Zhao 2008)

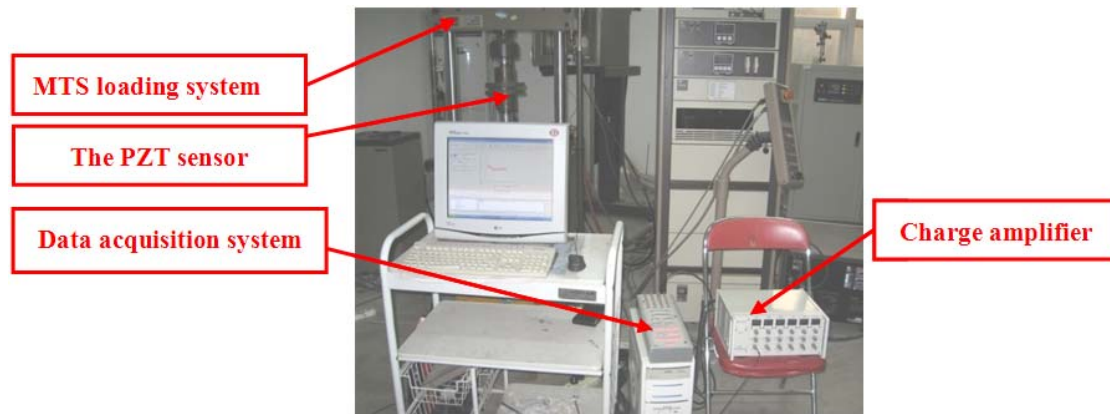


Fig. 9 Schematic diagram of calibration test (Zhao 2008)

2.3 Global positioning system receiver

The GPS satellite arrays were established by the Department of Defense aimed to determine directly the absolute position coordinates, and nowadays relative displacements can be measured at rates of 100 Hz and at millimeter level. In last decades, the GPS has become a useful tool for monitoring static, quasi-static and dynamic responses of infrastructures exposed to the temperature variation, gust-winds, or earthquakes (Yi *et al.* 2010a, Yi *et al.* 2013b). A complete GPS monitoring system is mainly made up of three parts: one reference station comprising a dual-frequency GPS receiver installed at a nearby “fixed” location, completing with mounting brackets, and battery backup for operation without power; One or more “rover” stations, comprising a pair of dual-frequency GPS receivers installed on existing masts attached to the infrastructure; and the control centre PC running the real-time monitoring software.

In designing a GPS-based monitoring scheme, the most important thing is the communication link between the control centre PC and GPS stations since to devise GPS receiver beyond the engineering disciplines. The communication link can be wired or wireless set according to the site conditions. Fig. 11 demonstrates 6 typical data communications solutions (Yi *et al.* 2009). In Fig. 11, the reference station features a high-precision Leica GRX1200 Pro GPS receiver and the rover station is equipped with a Leica GMX902 GPS receiver.

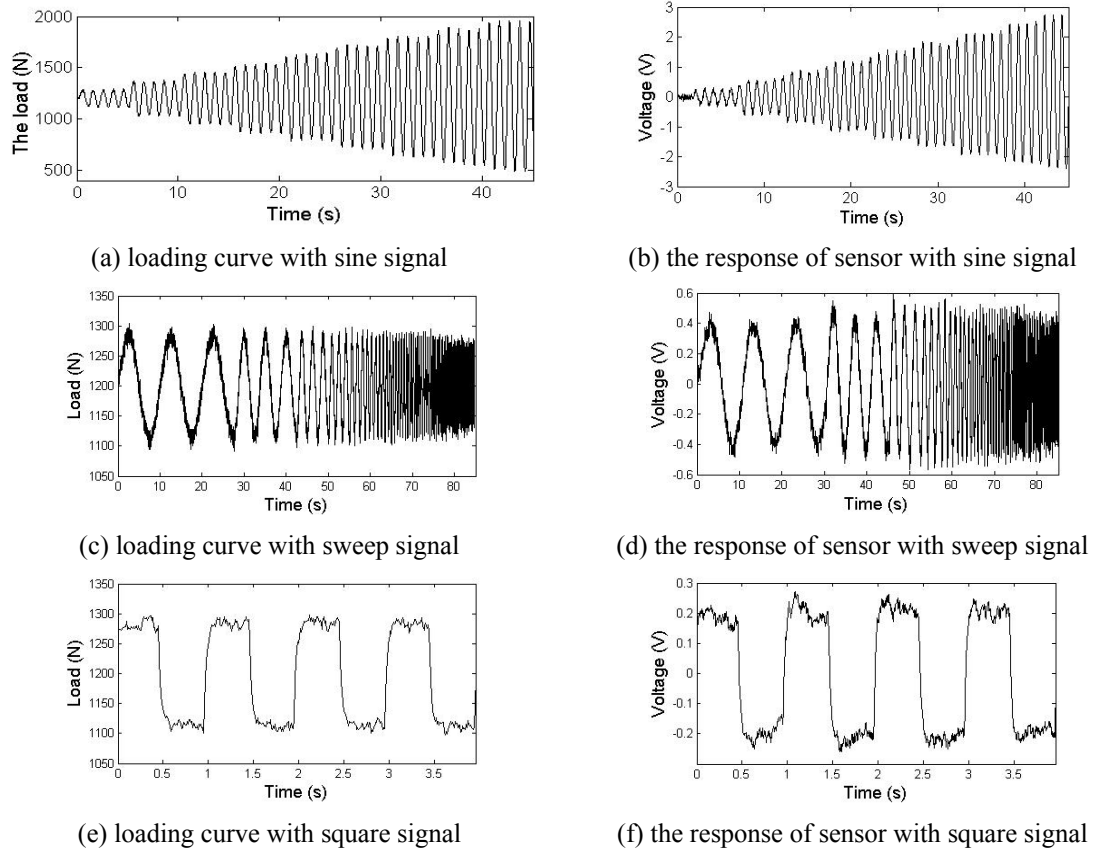


Fig. 10 Results of calibration test (Zhao 2008)

2.4 Polytypic and synchronous data acquisition device

In the field of SHM, more and more kinds of sensors have been applied to sense a number of physical measurement such as the FBG for the strain and electric sensors for the acceleration, pressure, displacement, inclination and so on. A critical demand for a general-purpose data acquisition device to synchronously measure a great amount of polytypic sensors has been proposed to satisfy requirements of data processing, calculation and structure analysis in some SHM projects. The general requirements for an ideal general-purpose data acquisition device are as follows: 1) high resolution with a large measurement range and high stability of wavelength measurement for the FBG interrogation; 2) high precision measurement and multiplicity of sensor types; 3) good synchronization of data sampling for both optical and electrical sensors; 4) robustness at the harsh environment.

A polytypic and synchronous data acquisition device system has been developed to measure the FBG sensors and electric signals, including voltage, current and digital I/O, which have covered most types of electric sensors. Fig. 12 shows a schematic diagram of polytypic and synchronous

data acquisition device.

This polytypic and synchronous data acquisition device, showed in Fig. 13, is featured with the following characteristics as listed in Table 2.

(a) A high-power, low-noise swept laser source for the FBG demodulation. Using a swept laser source instead of a broadband source yields many advantages such as greater distances to the FBG sensors (tens of kilometers) and multi channels functionality (up to 45), wide tuning range (80 nanometers) with more than 100 sensors per fiber, narrow source that provides better repeatability and accuracy (sub picometer), fast laser scanning for dynamic measurements (up to KHz), real-time built-in Calibration that means no periodic recalibration required.

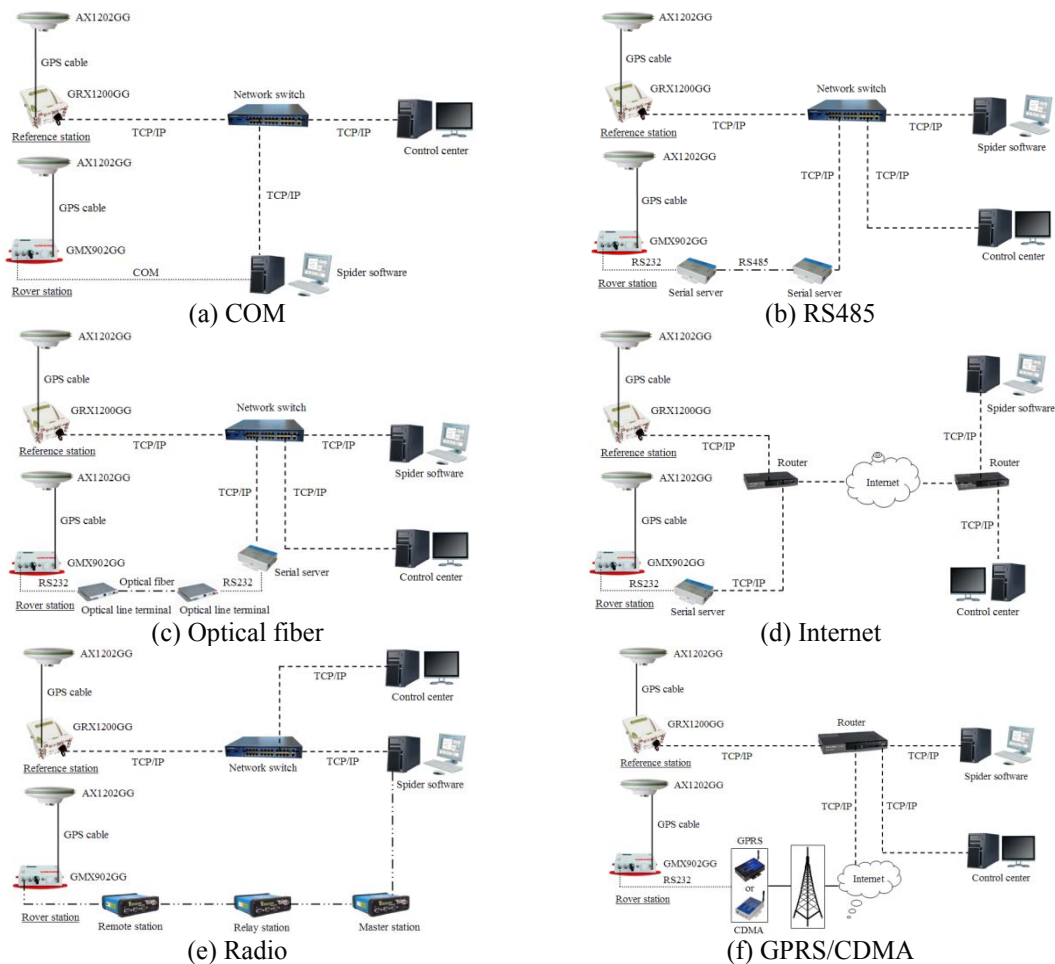


Fig. 11 Different GPS data communications solutions (Yi *et al.* 2009)

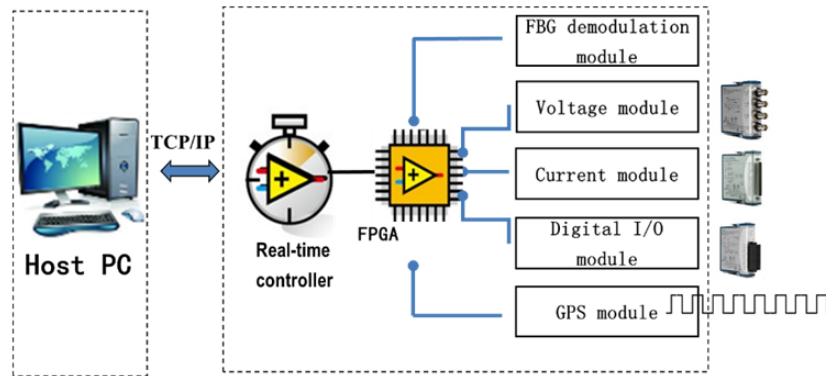


Fig. 12 Schematic diagram of polytypic and synchronous data acquisition device

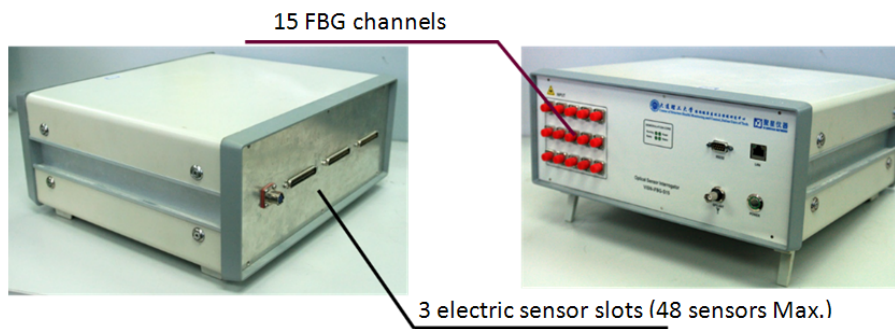


Fig. 13 Polytypic and synchronous data acquisition device

Table 2 The specifications of polytypic and synchronous data acquisition device

	Sampling rate	Resolution	Protocol	Bandwidth	FBG Channels	Electric sensors channels
iFBG-S15	2Hz	1pm	TCP/IP	80nm	15	48

(b) A synchronous data acquisition mechanism for polytypic signals. In this system, the signals from the FBG and electric sensors pass through the FBG demodulation module, voltage module, current module and digital I/O module respectively, which are controlled by the FPGA (Field Programmable Gata Array), as it is shown in Fig. 12. The FPGA, which minimize reliability concerned with the true parallel execution and deterministic hardware dedicated to every task, acts as not only the analog signals input unit to sense both FBG and electric sensors but also the synchronous timer with the 40MHz clock to trigger the signals sampling synchronously.

(c) An embedded hardware and real-time operating system with the industrial stability. The real-time controller contains an industrial processor that reliably and deterministically executes the data communication from the FPGA to host the PC and offers the multi-rate control for the data acquisition.

3. Basic theories and methods

3.1 Sensing technology

Although aforementioned sensors have been successfully applied to infrastructures to monitor relative displacements, cracks, and weight in motion as well as to measure strain and temperature, clear understanding of their operation principle, basic performance, data structure, etc., are essential to the monitoring data analysis and interpretations.

3.1.1 Optical fiber sensing technology

(1) Strain distribution along the fiber length of embedded OFSs

Conventionally, the values measured by the OFSs were assumed to be actual structural strains (Baldwin *et al.* 2002). In fact, the strain measured by an OFS is different from the actual host structure strain because of the difference between the optical fiber core modulus and the modulus of the fiber coating or the adhesive. Such a strain difference depends on the detailed packing measures of OFSs, for instance, the direct surfaced bonded, tube-or-plate packaged integration, or clamping integration as shown in Section 2.1. No matter how the OFSs are packaged or integrated, the fiber core is brittle and has to be protected by the adhesives or a coating layer to avoid fiber breakage and to ascertain its long term stability. Such protections result in inconsistency between the fiber strain and structural strain. The discrepancies, however, are neglected in many applications of OFSs by simply assuming that the fiber strain is consistent with the host structural strain (Friebele *et al.* 1999, Udd 1995). Such an assumption gives acceptable measurement results for the OFSs with a long gauge length, in which the peak host strain can be fully transferred into the fiber strain, but cannot provide good measurement strains for the short gauge OFSs, for instance, the FBG sensors, in which the effect of bonded fiber length on the strain transfer between the fiber and host structure is significant (Galiotis *et al.* 1984). It is, thus, of primary importance to reveal real relationship between the strain sensed by an OFS and the actual strain of the host material. Many researchers have made efforts in this field and obtained notable achievements. Pak (1992) analyzed the strain transfer of a coated optical fiber embedded in a host composite, which is strained by a far-field longitudinal shear stress parallel to the optical fiber. In this case, the maximum shear transfer occurs when the shear modulus of coating is the geometric mean of shear moduli of the fiber and host material. Ansari and Libo (1998) developed a simply model for evaluating the strain transfer percentage from the surrounding matrix to a length of optical fiber embedded in it under the assumption that the strain at the middle of the bonded fiber is equal to that of the host structure at the same position. Experiments were performed with a white-light fiber-optic interferometer to confirm the theory results. Li *et al.* (2002) considered the coating as an ideal elasto-plastic material and deduced the strain transfer coefficients when the host material experiences the tensile stress and compression stress respectively. Galiotis (1984) designed a polydiacetylene single fiber in an epoxy resin host material subjected to the tensile strain along the fiber direction, and measured the strains at all points along the length of fiber by the method of resonance Raman. They found that the axial strain in the fiber rises from a finite value at the end of fiber to a fairly constant value at the central portion of fiber, and that the axial strain at the midpoint of fiber is lower than that applied to the host material, which can be approximately explained by the shear-lag model of Cox (1952).

Recently, Li *et al.* (2005) derived the strain distribution along the fiber at a given x coordinate as follows

$$\varepsilon_g(x) = \varepsilon_m \left(1 - \frac{\cosh(kx)}{\cosh(kL)}\right) \quad (5)$$

Eq. (5) is the governing equation that describes the strain distribution along the fiber. The effects of the Young's moduli of fiber and the middle layer, as well as the effects of the radii of fiber and the middle layer, on the strain transfer, are all included. Fig. 14 shows the strain transfer rate along an optical fiber and demonstrates that the strain sensed by the fiber at the midpoint is not equal to the strain in the host material as previously assumed by Ansari and Libo (1998). For detailed derivation of Eq. (5), interested readers may consult Li *et al.* (2005).

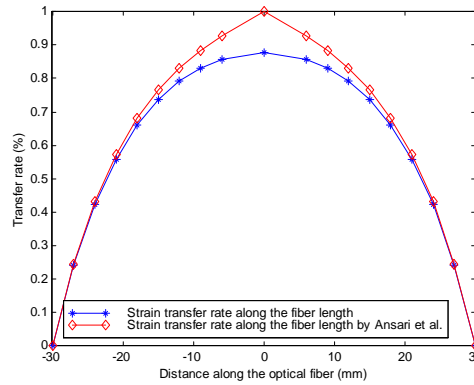


Fig. 14 Distribution of normal strain in fiber along length (Li *et al.* 2005)

(2) Average strain transfer rate of OFS and critical adherence length

The strain measured by an OFS, is the average strain over the gauge length of fiber. Average STR (ASTR) can be expressed in the following form

$$\bar{\alpha} = \frac{\bar{\varepsilon}_g(x)}{\varepsilon_m} = \frac{2 \int_0^L \varepsilon_g(x)}{2L\varepsilon_m} = 1 - \frac{\sinh(kL)}{kL \cosh(kL)} \quad (6)$$

Eq. (5) indicates that the STRs near the center of fiber approach unity and varies within the fiber gauge length. However, only a short portion of FBG sensor is usually bonded and the bonded length cannot be too short to avoid multiple-peak reflection and light spectrum expansion of FBGs. Critical adherence length (CAL) is thus defined as the minimum length to be bonded so that the STRs

$$CAL=l_c=9.24/k \quad (7)$$

where l_c is only computed over the half gauge length.

The critical adherence length means that an OFS can be bonded over a longer portion, and the effective gauge length is located in the middle. For the case of OFS shown in Fig. 14, its CAL is 99.78 mm. This implies that the STRs along the middle half-length of fiber are larger than 0.9 as

long as the minimum bonded fiber length is beyond 99.78 mm. The CAL indicates that an FBG can be bonded over a longer length, for instance 80 mm, to locate the FBG just in the middle of adhered length for the efficient strain transferring.

(3) Influence of the host material

Many experiments and interrelated investigations have revealed that the effects of host material properties on the strain transfer cannot be ignored because of local enhancement especially when the stiffness of host materials is much lower than that of fiber. In authors' previous investigations (Li *et al.* 2007, Li *et al.* 2009), an improved strain transfer model is developed considering the influence of host material. An additional assumption is that the normal stress and the shear stress are both existent in some range of host materials and the influencing radius is equal to four times the external radius of interlayer. The derivation is similar to the simple model and the final solution is in the same form as in Eq. (5) with the only exception that the shear lag parameter, k , takes a different expression as follows,

$$k^2 = \frac{2}{r_f^2 E_f \left\{ \frac{1}{G_c} \ln\left(\frac{r_c}{r_f}\right) + \frac{1}{G_m} \left[\frac{r_m^2}{r_m^2 - r_c^2} \ln\left(\frac{r_m}{r_c}\right) - \frac{1}{2} \right] \right\}} \quad (8)$$

(4) Strain transferring for a multi-layered concentric model

In many cases, there are several middle layers between the fiber and host material, for instance, the fiber is first coated with an adhesive that solidifies quickly, and then bonded to the structure by the epoxy that solidifies slowly to ensure a uniform stress distribution. One typical case is to bond the fiber to a structure by directly applying adhesives on the fiber coating, and the coating and the adhesive form two separate layers between the fiber and host material. In some sensing applications, specialized coatings are required to enhance an optical fiber's measurement sensitivity and to accommodate the host structure. The OFSs may be coated in this way with two different layers of coatings to employ their advantages of mechanical properties.

A multiple layer model with various middle layers is analysed in a similar way as aforementioned. r_i is the outer radius of the i th layer ($i=1\sim n$), r_g is the outer radius of the fiber layer, r_m is the inner radius of host materials (i.e. the outer radius of the $(n+1)$ th layer), G_i is the shear modulus of the i th layer ($i=2\sim n$), and G_c is the shear modulus of the 1st layer. The strain lag parameter k_m , similar to the formerly discussed case, is determined by the Young's moduli of fiber and the middle layers, and the diameters of fiber and the middle layers as

$$k_m^2 = \frac{2}{r_g^2 E_g \left\{ \sum_{i=2}^n \frac{1}{G_i} \ln\left(\frac{r_i}{r_{i-1}}\right) + \frac{1}{G_c} \ln\left(\frac{r_1}{r_g}\right) \right\}} \quad (9)$$

(5) Strain transferring mechanism for surface-bonded OFSs

Apart from embedded FBG sensors, the bonded FBG sensors are used more frequently. Because of the asymmetry of the bonded sensors system, the theoretical analysis is difficult. The research methods have concentrated on the computer simulation with the finite element model (FEM) mostly. Betz *et al.* (2003) studied strain transferring of patch bonded FBG sensors with the finite element analysis and experiments. The fiber is first placed on a backing patch and this patch

is simply glued to the surface of a structure. The thickness and the modulus of backing material are varied in the model. When the structure is strained with 0.3% parallel to the direction of fiber axis, the strain level in the fiber core is found to vary between 0.26%~0.28%. It is concluded that the structural strain has not been completely transferred due to the fiber due to the presence of backing patch, and that the degree to which the strain is transferred depends on the thickness and Young's modulus of backing. Lin *et al.* (2005) investigated three packaging methods of FBG sensors and found that strain transmission rates decreased with the increase in thickness of steel tube. Their experiments showed, however, that the thickness and Young's modulus of the glues had little influence on the strain transmission.

Li *et al.* (2008) and Zhou *et al.* (2010) found also that the strain transmission loss was small when the substrate is thick and stiff as compared to the bonding layer and the FBG. However, it becomes large when the substrate is thin and made by low modulus materials. Wan *et al.* (2008) studied the strain transfer with the stiff adhesive case with a 3D-FEM for a surface-mounted strain sensor verified it by experiments. They found that the bond length and the bottom thickness were dominant factors besides the side width and top thickness. Jahani and Nobari (2008) demonstrated that both Young's and shear moduli of adhesive were frequency dependent on dynamic testing because adhesive materials show the viscoelastic behaviour.

3.1.2 Piezoelectric sensing technology

The PZT based SHM techniques can be classified as the active and passive SHM methods. For the active technique, the piezoelectric patches are used as both actuators to excite the structure and sensors to accept the response signal. However, the passive method only uses the reception function of piezoelectric patches to receive the information of structures caused by damage.

The active PZT based SHM includes the electro-mechanical impedance (EMI) technique and the wave propagation-based technology. For the EMI technique, a PZT patch is bonded to the structure and a high-fidelity electro-mechanical admittance signature of patch serves as a diagnostic signature of structure (Liang *et al.* 1994). The electro-mechanical model of EMI is shown in Fig.15. Due to the sensitivity to small local damage, the EMI method has become a promising and attractive tool for the SHM. The EMI method has been applied to the crack detection of steel beam (Ritdumrongkul and Fujino 2007), damage evaluation of concrete structures (Bhalla and Soh 2003) and concrete strength development (Tawie and Lee 2010). For the wave propagation-based technology, arrays of surface-bonded or embedded piezoelectric patches are utilized to be transmitters and receivers of elastic waves. One of the most popular wave propagation technologies is the Lamb wave based method which is widely used in plates and shells structures. For the large scale of civil structure such as the concrete members, it is difficult to excite the desired modes of Lamb wave due to their large thickness. The stress wave propagation based technique has widely used in large scale infrastructures. The stress wave can be regard as the longitudinal wave or transverse wave, which is non-dispersive since their wave speeds are only a function of material properties. The principle of the method is shown in Fig. 16, in which one of the piezoelectric transducers is used as actuator to excite stress wave, and another one is used as the sensor to accept signals. The amplitude of the wave, which represents transmission energy, will decay rapidly due to the existence of cracks. The drop value of transmission energy will be correlated with the degree of damage inside. A type of damage index (Zhao and Li 2008a) based on continuous wavelet analysis is established as follows

$$D_I = 1 - \int_{t_0}^{t_1} |Wf_g(t, s_0)|^2 / \int_{t_0}^{t_1} |Wf_b(t, s_0)|^2 dt \quad (10)$$

where Wf_g and Wf_b express the wavelet coefficients of elastic wave in damage and healthy work conditions, respectively, t_0 and t_1 mean the start and end time of elastic wave propagation, respectively.

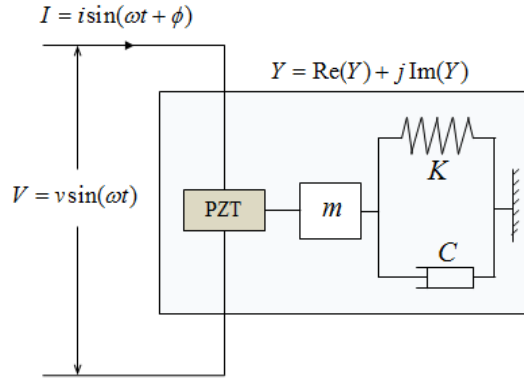


Fig. 15 Electro-mechanical model of EMI technique (Liang *et al.* 1994)

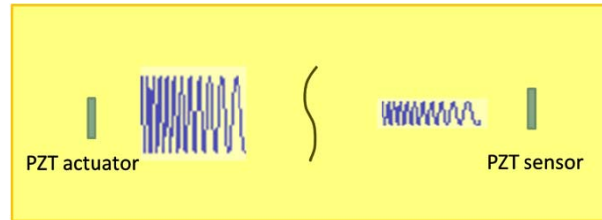


Fig. 16 Principle of stress wave propagation method (Zhao and Li 2008a)

In addition, the monitoring of crack development from reinforced concrete beams is conducted as shown in Fig. 17. Fig. 18 is the variation of damage index with the development of crack opening, which shows that the proposed damage index can correctly express the initiation and development of crack in the reinforced concrete beam.

For the passive SHM using the PZT, one of the most important applications is to identify the dynamic modal parameters of structures. Zhao and Li (2008b) embedded the PZT sensors into the concrete columns and beams with the vibration test. From the response of embedded PZT sensors, the modal frequency of concrete members can be clearly identified. In the vibration test based on the piezoelectric sensors, the beat phenomenon emerged in which the amplitude tended to decrease or increase periodically as shown in Fig. 19. Li *et al.* (2012) analyzed the cause of beat phenomenon in the piezoelectric sensors embedded in the simply supported concrete beam, and

revealed that the beat phenomenon was caused from the coupled modal responses with similar frequencies from the different direction.

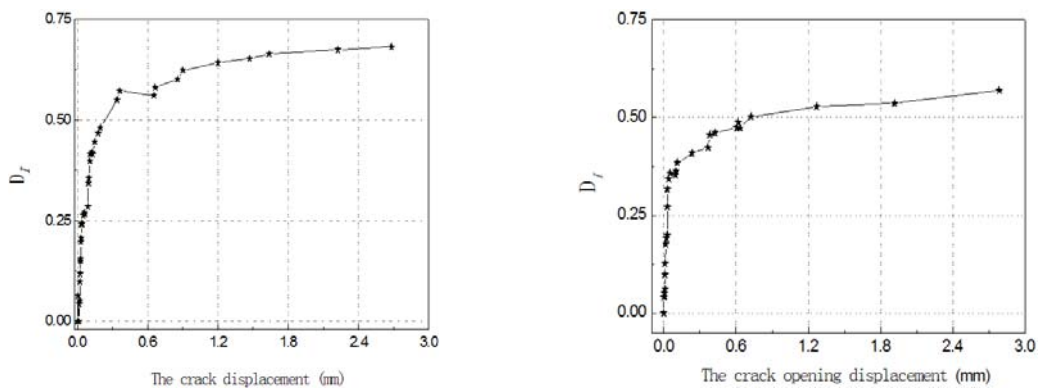


(a) Arrange of PZT sensors in reinforced concrete beam



(b) The diagram of the test

Fig. 17 Experimental photo of the crack monitoring test of reinforced concrete test (Zhao and Li 2008a)



(a) Damage index on the path from PZT-1 to PZT-3 (b) Damage index on the path from PZT-2 to PZT-3

Fig. 18 Variation of damage index with development of crack opening displacement (Zhao and Li 2008a)

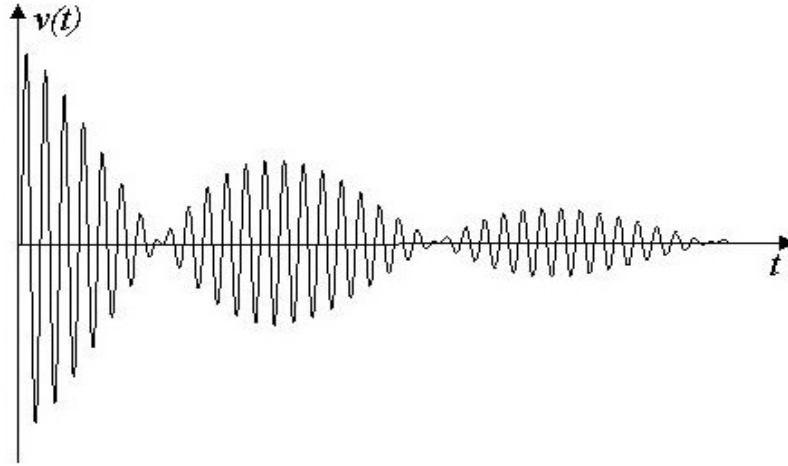


Fig. 19 Classical beat phenomenon from piezoelectric ceramic sensors (Li *et al.* 2008b)

Another application of passive SHM is to receive the acoustic emission signals caused by the inner crack of structures. Zhao (2008) conducted a comprehensive monitoring for the seismic damage experiment of a reinforced concrete frame-shear structure, in which the dynamic responses and acoustic emission signals were abstracted by the wavelet Mallat algorithm. The arrange of PZT sensors is shown in Figs. 20 and 21. Fig. 22 gives the modal frequency from the PZT sensors and acceleration sensors. The accumulative rings of acoustic emission in each sensor are shown in Fig. 23, which can illustrate the level of local damage.

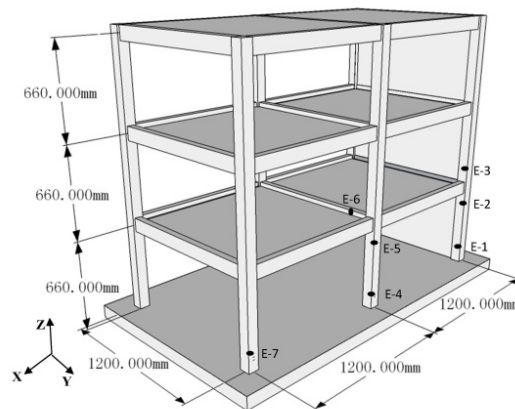


Fig. 20 Arrange of PZT sensors (Zhao 2008)



(a) The model of RC frame structures



(b) The sensor embedded in the column

Fig. 21 Experimental photos (Zhao 2008)

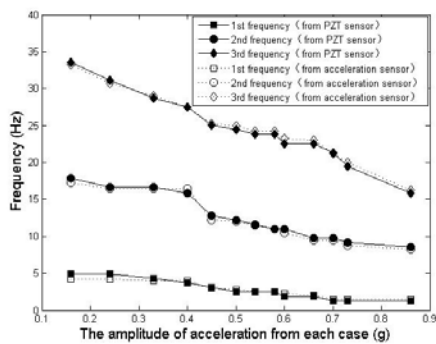


Fig. 22 Modal frequency from PZT sensors and acceleration sensors (Zhao 2008)

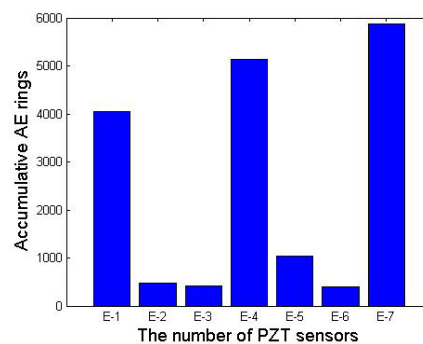


Fig. 23 Accumulative rings of acoustic emission in each sensor (Zhao 2008)

3.1.3 GPS sensing technology

As known, the double-differencing technique is commonly used for constructing the functional model as it can eliminate or reduce many of the troublesome GPS biases (i.e., the atmospheric biases, the receiver and satellite clock biases, and the orbital bias) (Li *et al.* 2007, Yi *et al.* 2010b). However, some unmodelled biases still remain in the GPS observations, even after such data differencing. The multipath is a major residual error source in the double-differenced GPS observables, and it can have a significant impact on the positioning results. In order to effectively mitigate the effects of multipath, it is necessary to have a detailed understanding of the signal transmitted from the satellite, reflection process, antenna characteristics and the way in which the reflected and direct signals are processed within the receiver. Yi *et al.* (2011b) established a model of GPS multipath propagation. By means of computer simulation, they found that highly reflective surfaces (to GPS signals) would lead to strong multipath signals (i.e. large amplitude), and objects close to the antenna would cause multipath signals with long wavelengths (conversely, distant objects usually cause multipath signals with short wavelengths). The key geometrical factor is the satellite elevation angle, with most reflected signals coming from nearby structures or the ground for a large incidence angle (Fig. 24). Most of these factors are closely related to the reflecting

environment. In order to systematically conclude the effects of different construction materials on the GPS signals, Yi *et al.* (2012b) devised a novel experimental set-up to test the effect of typical building surface materials on positioning accuracy (Fig. 25). They found that the wood board caused the smallest error to the positioning solutions, followed by the PVC board, ceramic tile, toughened glass, and aluminum plate. The amplitude of multipath signals arising from such reflections is highly dependent on the relative permittivity of medium, so do the standard deviation of multipath signals. It is also noted that the amplitude of multipath signals in three directions decrease with the increase of distances, and the decreased rate gets smaller. The changed rate of multipath signals in the vertical direction is about two times bigger than that in the horizon, and the multipath signals tend to be gentle along with the increase of distances in three directions. These meaningful findings of experimental results can be used to enhance the performance of GPS monitoring technology.

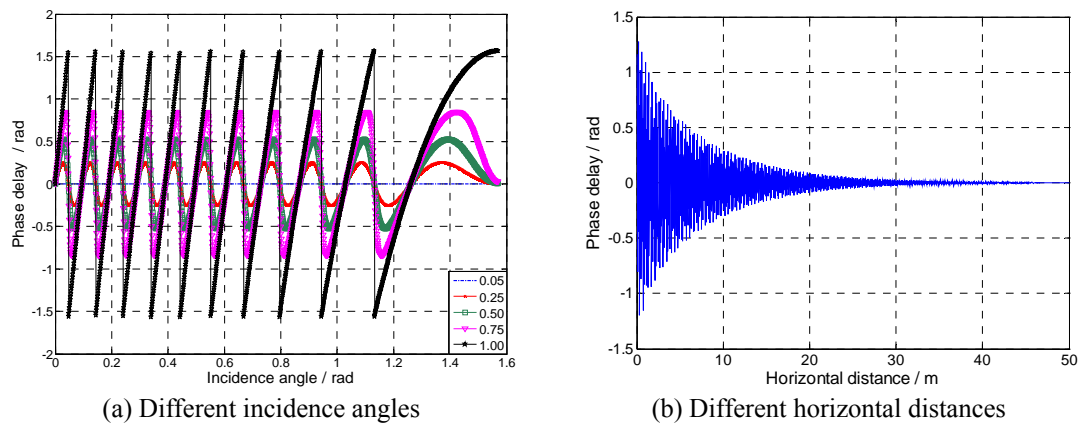
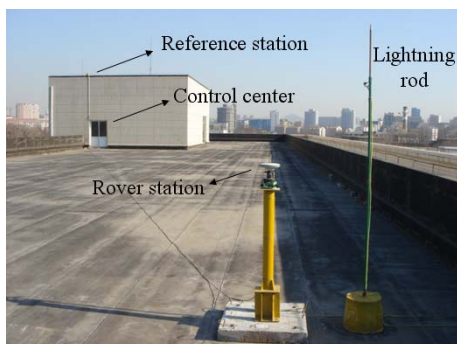
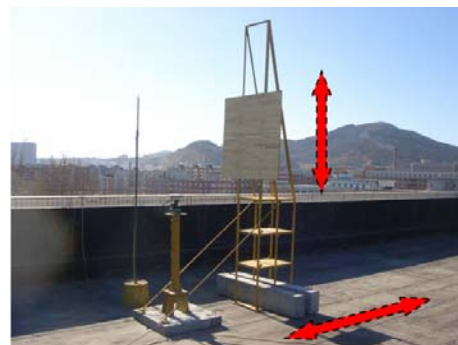


Fig. 24 Multipath signals corresponding to different incidence angles and different horizontal distances (Yi *et al.* 2011b)



(a) Configuration of GPS monitoring system



(b) Set-up of the reflector near the rover antenna

Fig. 25 GPS multipath signal generating experimental set-up (Yi *et al.* 2012b)

As known, the typical GPS receiver is only at a rate of up to 20 Hz that limits its capability in detecting certain high mode signals of some infrastructure. With the rapid advancements in available sampling rates and tracking resolution, the high logging rates GPS receivers have been emerged to the market. Yi *et al.* (2013a) systematically investigated the reliability and practicability of using high-rate carrier phase GPS receivers to characterize the dynamic oscillations of bridge. The receivers evaluated by them are the NovAtel ProPak-V3 which is capable of sampling data at up to 50 Hz, and the JAVAD TRIMMPH-1 which is capable of gathering data at up to 100 Hz (the highest sampling frequency in the market). The static, kinematic and on-site dynamic experiments are carried out to investigate the frequencies and amplitudes of the background noise of high-rate GPS receivers and reveal its potentiality to measure the rather stiff structures. As shown in Fig. 26, the high-rate GPS receiver can quantify both environmental induced bridge vibrations and high-frequency transient motion caused by the vehicle loading, providing the ability for verification and/or improvement of structural design and modeling.

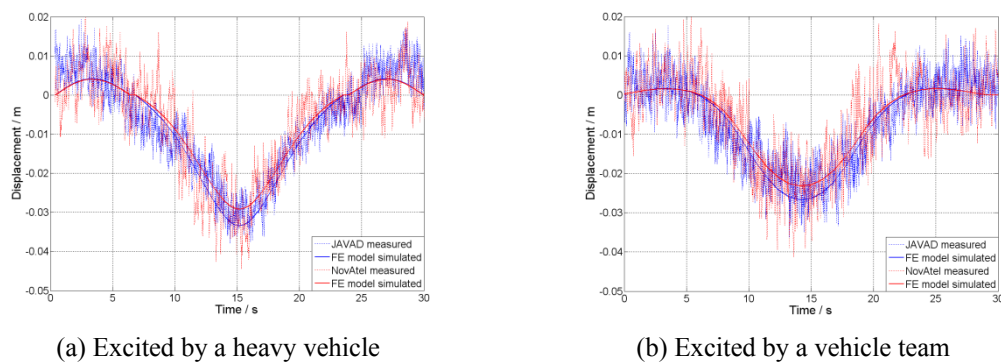


Fig. 26 Observed and modeled deflection in vertical direction at GPS site (Yi *et al.* 2013)

3.2 Sensor placement methods

Optimal sensor placement (OSP) technique plays a key role in the SHM of large infrastructures (Yi and Li 2012a, Yi *et al.* 2011a, Yi *et al.* 2013e). The issue of sensor placement attracts much attention from both academia and industry, especially due to the increased number of instrumented large structures for the health monitoring in the last decade (Balageas *et al.* 2006). The sensors installed in these structures are mostly permanent and are always sparse, in fact, far less than available positions (Farrar and Worden, 2013). This is partly because of economic reasons, high cost of data acquisition systems (sensors and their supporting instruments), partly because of structural accessibility limitations. Furthermore, the wiring of sensors leading to monitoring room requires non-interfere routing and special care to prepare their integrity, particular for the optical fiber sensors (Li *et al.* 2004). Although wireless sensors are coming into use, the time synchronization and routing protocol problems currently limit their wide applications. Consequently, how to optimally deploy the limited number of sensors for better structural identification and feature extraction is a challenging task. The positioning of sensors can be approached from various aspects and many methodologies have been developed, for instance, the modal kinetic energy method (MKE) (Papadopoulos and Garcia 1998), model reduction based

methods (Penny *et al.* 1994), effective independence (EI) method (Kammer 1991 and Tinker 2004), MinMAC algorithm proposed by Carne and Dohrmann (1995), equidistant point selection method based on the Shannon's sampling theorem in a space domain (Stubbs and Park 1996), space sampling method based on the Chebyshev polynomials (Limongelli 2003), methods based on the mutual information (Trendafilova *et al.* 2001), and information entropy (Papadimitriou 2004).

3.2.1 Placements theory

Recently, Li *et al.* (2007) discovered the connection between two influential methods, the EI and the MKE. The EI requires iteration computations, but the MKE not. In the iterations of EI, it redistributes the modal kinetic energy into the retaining DOFs and recomputed their MKE index for the reduced system using re-orthonormalized mode shapes. In this sense, the EI is an iterated version of MKE with re-orthonormalized mode shapes. Afterwards, Li *et al.* (2009) proposed a new computation scheme of EI though the QR downdating. In the new scheme, the EI is computed with reduced modal matrix after a row is removed from the previous modal matrix and on the direct comparison of row norms of decomposed orthonormal matrix by the QR decomposition. Furthermore, the QR decomposition downdating steps based on the combination of the modified Gram-Schmidt and Householder transformations are implemented and further improve the EI computation efficiency considerably by eliminating the unnecessary costly QR decompositions in the EI iterations.

Existing sensor placement methods share a common feature, which is that sensor positions are solely determined provided that mode shapes of a structure are known. No matter what responses a structure will undergo, the final selected sensor positions are the same and don't take actual structural responses into consideration. Recently, Li *et al.* (2012) proposed a novel load dependent sensor placement (LDSP) method based on a newly proposed representative least squares method. The proposed LDSP method allows consideration of degree to which an individual mode shape participates in actual structural responses with a new objective function called nearly global unbiasedness criterion as follows,

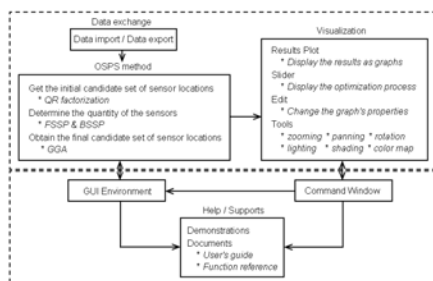
$$\mathbf{J}_{gu} = (\hat{\mathbf{q}}_s - \hat{\mathbf{q}}_{OLS})^T (\hat{\mathbf{q}}_s - \hat{\mathbf{q}}_{OLS}) \quad (11)$$

where \mathbf{J}_{gu} is the objective function, $\hat{\mathbf{q}}_s$ is the OLS estimator with the same subset of s components in both Φ and \mathbf{y} (required s sensor positions, selecting s out of n rows) and $\hat{\mathbf{q}}_{OLS}$ is an OLS estimator with all n components (all n candidate sensor positions). Under the nearly global unbiasedness criterion as defined in Eq.(11), it is strived to choose a given number of sensor positions that map the mode shapes of interest to actual structural responses as closely as possible. In other words, structural responses will fall into the space spanned by the mode shapes as much as possible. Therefore, the proposed method depends on both the characteristics and actual loading situations of a structure. It selects sensor positions with the best subspace approximation of vibration responses from the linear space spanned by the mode shapes. When the solution of the LDSP method is implemented in a sub-optimal sense, the objective of the LDSP method agrees exactly with the criterion used by the EI. Furthermore, the LDSP method searches the minimum change of its original condition number of design matrix with combinational rows in a global sense, whereas the EI tracks the minimum change of condition number in each of its iterations. Therefore, the LDSP method can be regarded as a generalization and extension to the most influential EI method.

3.2.2 Intelligent algorithm

The aforementioned analyses have shown that the general sensor selection problems addressing the diagnosability, observability, reliability, or detectability are NP complete and are therefore computationally intractable. These types of issues require efficient searching solutions in order to generate acceptable results in reasonable time. In the recent years, combinatorial optimization methods based on the biological and physical analogue have been extensively used for the optimization of OSP problems due to their many advantages over the classical optimization techniques such as they are blind search methods and highly parallel.

There are many interesting intelligent algorithms to tackling sensor placement problem, but one of the most powerful heuristics is based on the genetic algorithms (GAs). The GA has many drawbacks, such as it may spend much time on complex optimization problems. Yi *et al.* (2012c) proposed a kind of improved generalized genetic algorithm (GGA). In this improved GGA, the dual-structure coding method instead of binary coding method was proposed to code the solution. Accordingly, the dual-structure coding based selection scheme, crossover strategy and mutation mechanism are derived. To demonstrate the feasibility and effectiveness of the improved GGA, the sensor placements obtained by it are compared with those by the exiting simple GA (SGA), which shows that the improved GGA can improve the convergence of the algorithm and get the better placement scheme (Yi *et al.* 2011c). Based on these results, a hybrid method termed the optimal sensor placement strategy (OSPS) based on the multiple optimization methods is proposed by Yi *et al.* (2011d). In this approach, the initial sensor placement is firstly obtained by the QR-factorization. Then using the minimization of the off-diagonal elements in the modal assurance criterion (MAC) matrix is as a measure of the utility of a sensor configuration, and the quantity of the sensors is determined by the forward and backward sequential sensor placement (SSP) algorithm together. Finally, the locations of sensor are determined by the improved GGA. Taking the scientific calculation software MATLAB as a platform, an OSPS toolbox, which is working as a black box, is developed based on the command-line compiling and GUI-aided graphical interface design, as shown in Fig. 27. The characteristic and operation method of toolbox are introduced in detail and the scheme selection of the OSP is carried out on the world second tallest TV tower – the Canton Tower based on the developed toolbox. In addition, Zhou and Yi (2013b, c) implemented the improved GGA to the non-uniform node configuration of wireless sensor networks (WSN) for a long-span bridge health monitoring. The simulated results verified that the proposed node arrangement method could balance the energy consumption, increase the data capacity and reduce the deployment cost.



(a) Functional block diagram



(b) Main window

Fig. 27 MATLAB software based OSPS Toolbox (Yi *et al.* 2011d)

Monkey algorithm (MA) is a swarm intelligence optimization algorithm which was designed by Zhao and Tang (2008) from the inspiration of mountain-climbing processes of monkeys. Yi *et al.* (2012d, e) first adopted the MA in the field of sensor placement. Based on substantial improvements on the original MA, they presented a series of novel improved MAs for the sensor placement, including the simple monkey algorithm (SMA), asynchronous-climb monkey algorithm (AMA), distributed monkey algorithm (DMA), immune monkey algorithm (IMA), virus monkey algorithm (VMA), niching monkey algorithm (NMA), adaptive monkey algorithm (AMA), and collaborative-climb monkey algorithm (CMA). These improved MAs can be adopted to the various infrastructures that have different requirements. For example, the DMA outperforms the conventional algorithms both in terms of generating optimal solutions as well as faster convergence; the NMA can enhance the exploitation capability effectively.

3.3 Signal processing and data fusion

With a great amount of long-term SHM systems designed and implemented in worldwide on infrastructures, a vast ocean of information relevant to the structural responses and behavior are continuously obtained in real time (Ran *et al.* 2012, Ye *et al.* 2012). The measurement data are valuable in detecting structural anomalies and damage at an early stage to ensure operational safety, and providing authentic information for timely assessment after disasters and extreme events. In view of this, the intelligent information processing technology, which is a process of transforming the incomplete, imprecise, inconsistent and uncertain information into complete, precise, consistent and certain information, should be developed.

3.3.1 Signal de-noising method

In on-site monitoring, one of main factors which disturb the reliability and accuracy of results is the noise signals encountered. The noise embedded in useful signals, sometimes even very heavy, could disturb the reliability and accuracy of measurement, and thus places a fundamental limit on the detection of small defects. Thereby, the noise reduction should be treated as an essential processing in the SHM.

The wavelet transform (WT), due to it capable of revealing some hidden aspects of the data that other signal analysis techniques fail to detect, has become a potential tool in recent years (Li *et al.* 2009a). To get over the disadvantages of the traditional hard- and soft-thresholding method in the WT based denoise method, Yi *et al.* (2012f) proposed an improved thresholding technique called the sigmoid function based thresholding scheme. Fig. 28 illustrates the comparison with the soft, hard and sigmoid function based thresholding scheme. Numerical and experimental results have demonstrated that this technique can remove small coefficients and shrink large coefficients using its non-linear characteristics to reproduce peaks and discontinuities as accurately as possible without sacrificing visual smoothness. Considering that the GPS multipath signal exhibit the same pattern between consecutive days, Yi and Li (2006) designed an integrated method based on the adaptive noise cancelling (ANC) principles and discrete wavelet denoise method. On the site experimental data analysis results indicated that the error of standard deviation of the GPS signal could be reduced less than 5%. In addition, Yi *et al.* (2013c) carried a study on how to use the GPS receiver and accelerometer data to accurately extract the static and quasi-static displacements of bridge induced by ambient effects. To eliminate the disadvantages of two separate units, based on the characteristics of bias terms derived from the GPS and accelerometer respectively, a wavelet based multi-step filtering method by combining the merits of the continuous wavelet transform

(CWT) with the discrete stationary wavelet transform (SWT) is proposed, as shown in Fig. 29. Experimental results showed that the frequencies and absolute displacements of bridge could be accurate extracted by this method.

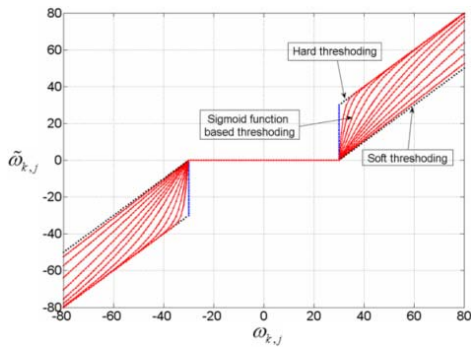


Fig. 28 Comparison of soft, hard and sigmoid function based thresholding scheme (Yi *et al.* 2012f)

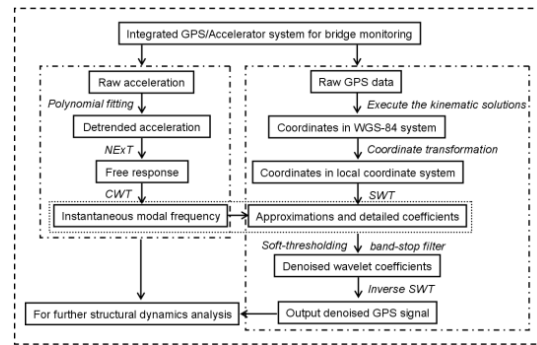


Fig. 29 Flowchart of the proposed multi-step filtering method (Yi *et al.* 2013c)

3.3.2 Data fusion technique

To reduce the uncertainty, imprecision and low reliability, the multi-sensor data fusion technique had better to be adopted. Jiao and Li (2006) proposed an improved data fusion method based on the consensus algorithm for a multi-sensor system. In this method, the relation matrix is innovatively blurred to avoid the subjective error in determining the threshold value. Lai *et al.* (2010) presented a multi-rate Kalman filtering data fusion method for the displacement and acceleration data based on the Wiener process acceleration model, which exploits the inherent redundancy in the displacement transducer and accelerometer information so as to improve the accuracy of vibration test data. Despite the vibration-based structural damage detection methods have attracted considerable attention over the past decade, the robust and reliable methods capable of detecting, locating and estimating damage whilst being insensitive to changes in environmental and operating conditions have yet to be agreed upon. Li *et al.* (2009b) developed an analytical approach for the seismic ground motions by applying the CWT, which focuses on the energy input to the structure. A scale model with a three-storey reinforced concrete frame-share wall structure is made and tested on a shaking table to investigate the relation between the dynamic properties of structures and energy accumulation and its change rates during the earthquake. The results showed that the proposed approach was able to provide a deep insight into the identity of transient signals through the time-frequency maps of time variant spectral decomposition. Considering that the wavelet packet transform (WPT) has the ability to clearly reflect the damage characteristics of structural response signals and the artificial neural network (ANN) is capable of learning in an unsupervised manner and of forming new classes when the structural exhibits change, Yi *et al.* (2013d) proposed a multi-stage structural damage diagnosis method by using the WPT and ANN based on the “energy-damage” theory, in which, the wavelet packet component energy is first

extracted to be damage sensitive feature and then adopted as the input into an improved back propagation (BP) neural network model for damage diagnosis in a step by step mode. The numerical results of damage diagnosis indicated that the method was computationally efficient and able to detect the existence of different damage patterns.

3.4 System identification and damage detection

3.4.1 A local damage detection approach based on restoring force method

A chain-like system identification approach was originally developed to identify modal parameters and restoring forces of the Factor building (Nayeri *et al.* 2008), and later was generalized to change the detection of chain-like system (Hernandez-Garcia *et al.* 2010). In the conventional restoring force method, the external forces are required to be known, which is not practical for some large-scale structures. Nayeri *et al.* (2008) extended the work of Marsi *et al.* (1982) by generalizing the restoring force method to handle the case of chain-like multiple degrees of freedom (MDOF) dynamic systems with unknown (immeasurable) external forces. The external force term in the chain-like system is eliminated by assuming that the unknown force is a stationary white noise process by computing the cross-correlation function with a reference acceleration time history combining with the natural excitation (NexT) technique (James *et al.* 1993, 1996).

However, some shortages still exist in that approach, and for overcoming them, we proposed an improved approach (Zhan *et al.* 2013). In this approach, only measured acceleration signals at each DOF are required, and the state variables, i.e., the velocities and displacements, are reconstructed by passing the measured acceleration signals through an finite element method finite impulse response filter. The mass normalized stiffness coefficients are estimated by the least square method. By analyzing the changes of mass normalized stiffness coefficients between two structural states, damages due to relative structural (stiffness and mass) changes can be identified. The proposed improvement can not only detect, locate structural changes, but quantify the degree of changes despite modeling, measurement and data processing uncertainties. The improved approach has many merits, and the most intriguing one is that the relative stiffness and mass changes, which are coupled in the previous approach, can be separately identified. By our approach, the damage (single or multiple) extent and location can both be correctly detected under operational conditions, meanwhile the proposed damage index has a clear physical meaning and is directly related to the stiffness reduction of corresponding structural elements.

3.4.2 Damage detection based on combination of successive displacement curvature under varying environmental temperature

Static displacement curvature of a structure could be used for the damage detection. However, it will also be influenced by varying environmental and operational conditions. Based on the unique characteristics of the curvature of a beam, we proposed a new damage identification index, i.e., the combination of successive displacement curvature (Liang *et al.* 2014). The position coordinates of three successive nodes of a beam bearing concentrated loads, and consequently their corresponding curvatures, satisfy certain relationship. Once the relationship fails to meet the relationship, damage occurs and thus can be identified.

Furthermore, influence of ambient temperature variation on the proposed damage index can be eliminated since successive displacement curvature bear similar trend under the same temperature condition, which is also the rationale of the so-called co-integration. Therefore, our method could

eliminate the influence of changing environmental temperature without the structural data in a healthy condition, and has the ability to monitor and identify the damage location online. For details of the proposed method, interested readers may consult Liang *et al.* (2014).

4. SHM Codes and Standards for Infrastructure

The application of promising SHM research to real-world operational infrastructures often fail because of a lack of standardization of SHM principles and best-practices. There is no doubt that the work of SHM standardization is particular challenging as every infrastructure is a prototype and the usual code applied to other sectors do not bring the desired success in this field. On the other hand, creating and implementing codes and standards are a time consuming process and not always in perfect alignment with priorities of research community. Fortunately, in the past decade, the entire SHM community spanning from researchers to end-users have acknowledged the importance of codes and standards in accelerating the adoption of SHM technologies. In some respective conferences and symposia (such as International Conference on Structural Health Monitoring of Intelligent Infrastructure (SHMII) hold by the International Society for Structural Health Monitoring of Intelligent Infrastructures (ISHMII), International Workshop on Structural Health Monitoring (IWSHM) organized by the Stanford University) prominent spaces are reserved where the community meets and discuss the progress and the roadmap for future development.

4.1 Activities on standardization of SHM

Five guidelines including “Intelligent Sensing for Innovative Structures (ISIS)” (Mufti, 2001), “Monitoring and Safety Evaluation of Existing Concrete Structures: State-of-the-Art Report (Fib)” (Bergmeister *et al.* 2002), “International Organization for Standardization (ISO)” (ISO 2002), “Federal Highway Administration (FHWA)” (Aktan and Catbas 2002), and “Structural Assessment, Monitoring and Control (SAMCO)” (Ruker *et al.* 2006) have been recommended by the ISHMII in 2007. Table 3 demonstrates the comparison between these five guidelines.




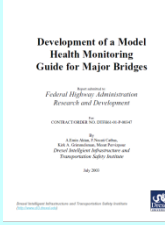

4.2 Design standard for structural health monitoring

The first standard in the area of SHM in China, *Design Standard for Structural Health Monitoring Systems* (CECS 333: 2012), was approved by China Association for Engineering Construction Standardization and started into use since 1st March 2013, as shown in Fig. 30. Coordinated by Prof. Li at Dalian University of Technology for three years, the Standard is co-authored by scholars and practitioners from Dalian University of Technology, Dalian Jinguang Construction Group Ltd, Southeast University, Harbin Institute of Technology, Beijing University of Technology, The Hong Kong Polytechnic University, and Hohai University in China. The Standard has been widely circulated among practitioners and researchers in China after putting it in force (Design code 2012).

The Standard consists of seven chapters, two annexes, and explanations. The main contents include: 1) General; 2) Definitions (Terms; Notations); 3) Sensor Selection and Placement (Sensor selection; Principles of sensor placement; Sensor placement method); 4) Data Acquisition and Processing (Data acquisition; Data processing); 5) Data Transmission (Design requirements; Quality control; Other requirements); Data Storage and Management (Functions and design

principles of database system; Basic requirements of database design; Configuration of database; Requirements of database selection; System interactive pattern; Operation and management of database); 6) Structural Condition Identification and Assessment (Modal parameter identification; Damage identification; Condition Assessment).

Table 3 Comparisons between different guidelines (Hejll 2007)

Guideline					
	ISIS	Fib	ISO	FHWA	SAMCO
Year	2001	2002	2002	2003	2006
Focused on	SHM Overview	Measurements	Vibration monitoring	Road Bridges	SHM
General	Concise; Easy to understand; Short case studies	Extensive; Covers most part of the SHM; Instructive case studies	Well focused; Only dynamic monitoring	Extensive; Well structured	Easy to understand; Well structured; Sensor classification; Separate assessment
Strategies					
Condition	Damage detection levels are discussed	Structural phenomena are presented	Only damage detection and localization are discussed	Phenomena and suitable monitoring parameters are discussed	Damage detection and Global monitoring is discussed.
Time	Static- and Dynamic field tests; Periodic- and Continuous monitoring	Time Scheduled and Sampling strategies are divided in Continuous and Periodic monitoring	Time dependent strategies are discussed	How the phenomena should be monitored regarding time are discussed	Sensors characteristics for long-term monitoring is presented
Load	Static and dynamic monitoring are discussed	Proof load tests and dynamic tests are presented	Discussion of excitation methods is present	Divided in Proof testing and dynamic monitoring	The guideline is divided in Static and Dynamic measurements
Evaluation	Not discussed	Mentioned in the introduction	Focused on vibrations, not safety	Not discussed	Separate Guideline

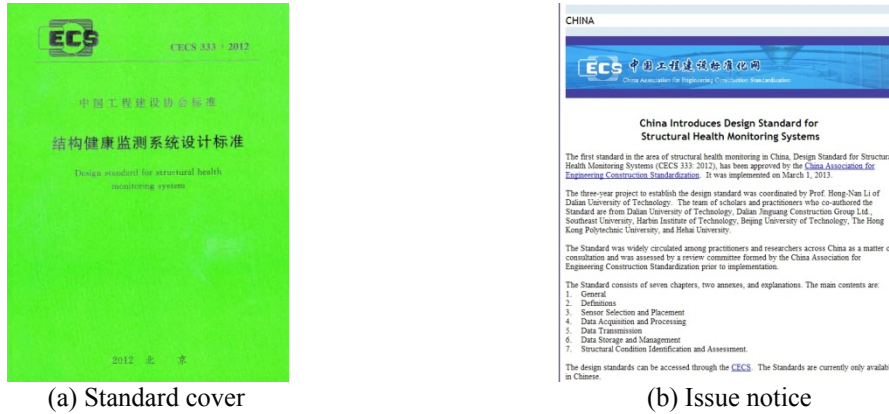


Fig. 30 Design Standard for Structural Health Monitoring Systems

5. Typical infrastructure applications

It has been shown that advances in sensing systems, signal processing, communications and data-mining technology are providing a new way for the inspection and monitoring of infrastructure safety. The following typical examples demonstrate some successful implementations of long-term SHM systems on different infrastructures carried out by the RCSHMC.

A sophisticated software system for structure health monitoring should satisfy the following demands: 1) sampling data continuously in real-time; 2) Compatibility with different type of sensors; 3) Steady data storage methods for the static and dynamic data; 4) Auto-warning functions; 5) Data analysis automatically. A special software architecture, named with the DUT-SHM, integrated by the state machine and event-driven architecture and featured with the functions of modularization and multithreading, was designed for the demands of structure health monitoring. Based the DUT-SHM architecture, the software system of SHM composed of the following software modules: 1) Data acquisition engine which functioned as data transferring based on the FIFO mechanism between the real-time device and FPGA module; 2) Network communication engine which submit the control command from the host PC to the real-time device and receive the data vice versa; 3) Data storage engine which save data in the real-time according to the different demands and data types; 4) Data display engine, which not only display the data by the chart and the 3D real-time model, but also provide several ways to send the warning information including the Email and the short messages to a cell phone; 5) Data analysis engine for the data automatic processing in a regular time; 6) Debug engine which served as the log writer and system monitor for the system error and state. Fig. 31 describes the functions and the operating mechanism of the software system of SHM and the Fig. 32 shows the software interface of SHM for the Dalian gymnasium.

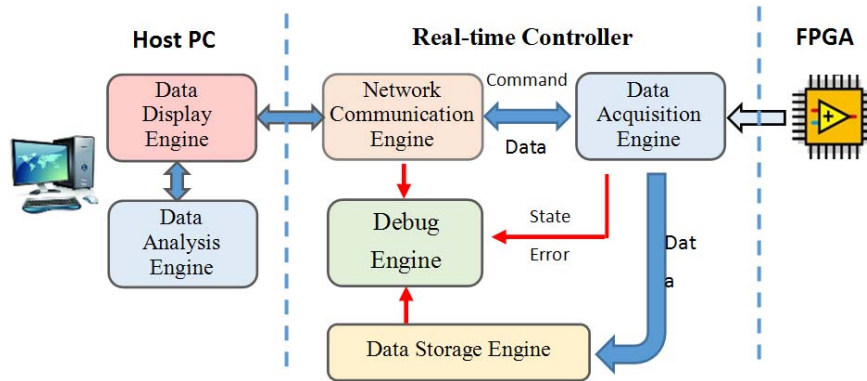


Fig. 31 Functions and operating mechanism of software system for SHM

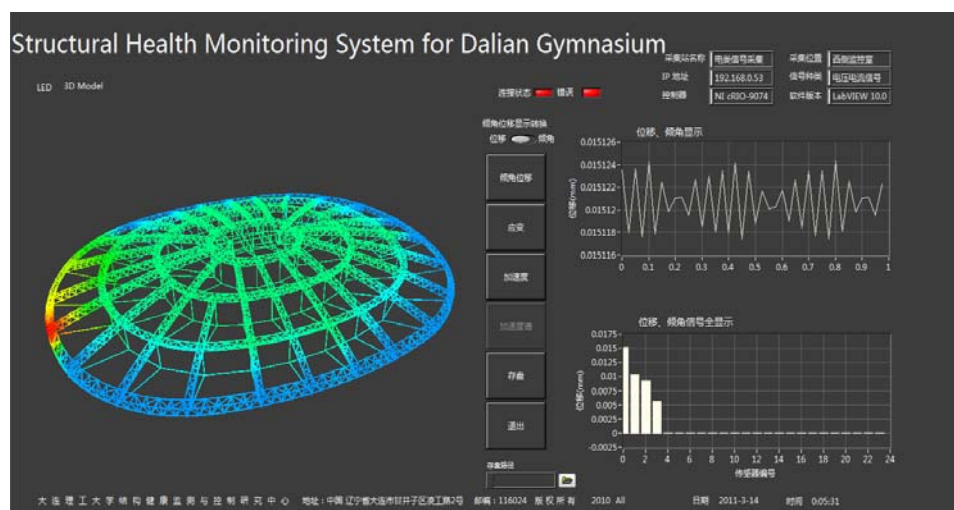


Fig. 32 Software interface of SHM system for Dalian gymnasium

5.1 Large-span structures

Recent years in China, a large number of long-span special structures have been built such as bridges, airport terminals and gymnasiums along with the development of special structure technique and material. These structures, other than suffering from natural hazards like earthquake and storm, are supposed to be subjected to vibrations caused by human factors (thousands of people jumping with the rhythm of music, for example). Nonetheless, aesthetically appealing from an architectural point of view, more recent structures are much lighter, with relatively low first natural frequency and significant motion amplitudes (Cigada *et al.* 2010). Huge casualties and financial loss would come about if the structure becomes invalid or even collapses. It is now more

and more urgent to conduct real-time monitoring system and damage diagnosis on the long-span special structures (Li and Li 2002). A big amount of data collected by the SHM system in real time, through certain damage algorithm, will offer a chance to estimate the security of structure and find out location of damage (Li *et al.* 2008).

Sports center of Dalian in China, which covers an area of 820 thousands square meters and composes of ten venues as shown in Fig. 33, is a comprehensive center of facilities of fitness and recreation for the Dalian citizens and has the capability of hosting major sporting events. The major buildings including the gymnasium, stadium, natatorium and media center, which are typical long-span special structures, were equipped with the real-time SHM system to survey the variation of key physical parameters of structures and provide the real-time alert of structural safety.

The overall floorage of Dalian gymnasium is about 81000m², which allows for 18000 spectator capacity with total height of 41 m. The roof structure of which the maximum span is 145.4 m is suspensome structure and shaped like a spheroid. These rings are designed for the prestressed cable system which is consisted of ring cable, radial cable and strut, while the strut made of circular steel tubes adopts the hinged joint and cast steel joint is applied between the cable system and strut. The location of maximum stress was found out based on the FE model results from the ANSYS software as it is shown in Fig. 34. More than 200 FBG sensors were installed on the cable anchor, the truss and the strut to monitor the cable force, the stress and the compression stress respectively. The 24 inclinometers were mounted on the base of cable anchor to monitor the angular variation. The 30 accelerometers with three dimentions were fixed on the surface of truss joints to survey the dynamic characteristics of the roof structure. The Fig. 35 shows the pictures of sensors installed on the roof structure of gymnasium.



Fig. 33 Pictures of Sports center of Dalian in China

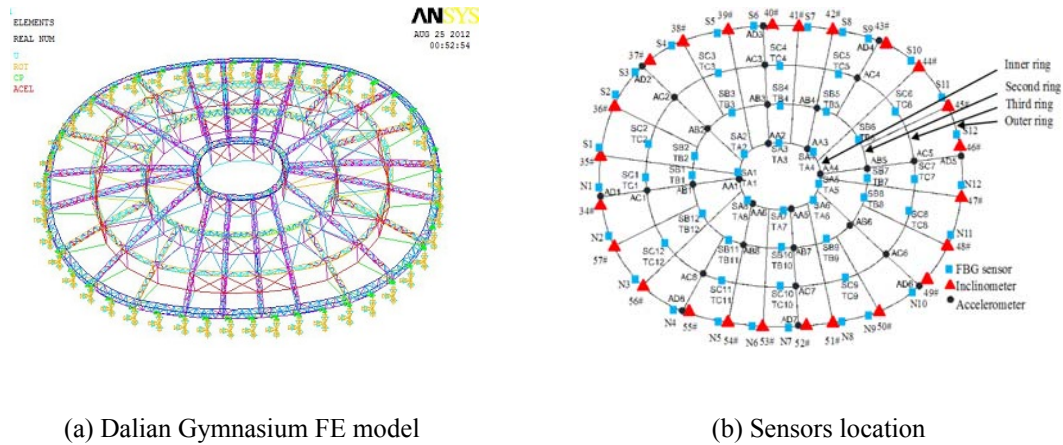


Fig. 34 FE model and sensors location



Fig. 35 Pictures of sensors installed on structure of gymnasium

(1) Monitoring results of cable system in the prestressing construction

Proper prestress on the radial cable can enlarge the stiffness of the cable system such that the structure would have the ability to undertake external load. Radial cable was tensioned during the construction of the prestressed cable. The whole process was divided into 4 stages: 10%, 50%, 70% and 105% of designed value respectively. In consideration of the quantity of equipment, each stage was carried out group by group to ensure the uniformity of tension. The tension construction lasted for 9 days in the process of which the above system was used to monitor the structure. Parts of monitoring results are listed as followed.

(a) Monitoring results of ring cable

The time-history of C10 cable tension during stretching process is shown in Fig. 36. During the first stretching process, the tension of C10 increased from 80 kN to 359 kN. There was a mutation in the process which was caused by the temperature change of sensor as a result of which the temperature compensation was necessary for the sensors.

(b) Monitoring results of strut

The stress time-history of Z1-2 strut in second stage of cable tensioning is given out in Fig. 37. In the process of the first stretching stage, the strut pressure stress has increased by 12MPa and 5 Mpa during the second stage, because the first stage prestress was directly applied to the radial cable connected with the strut Z1-2 and the second stage prestress was applied to the adjacent

radial cable. As a result, the effect of interaction between contiguous cables on strut was significant.

(c) Monitoring results of inclination

The inclination of 34# support increased from -0.888° to -0.851° , which was within the limit $\pm 1.5^\circ$, indicating that the structure was under safe condition, as is shown in Fig. 38.

(2) Long-term monitoring results

The monitoring system was switched on from the beginning of prestress construction. Part of the long-term monitoring results acquired by analysis of the monitoring data are as follows.

(a) Long-term monitoring results

The FBG sensors were installed on the key chord members as shown in Fig. 34. Fig. 39 shows the strain variation of parts of chord members from late August to early December in 2013. There was nearly no strain variation from August to October. When it came to November and December, the strain was enlarged due to the weight of equipment installed for the concerts and drastically falls in temperature which caused the structural shrinkage inducing the change of strain.

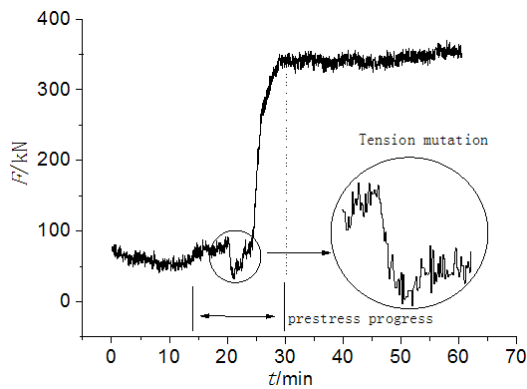


Fig. 36 Time-history of C10 cable during prestressing process

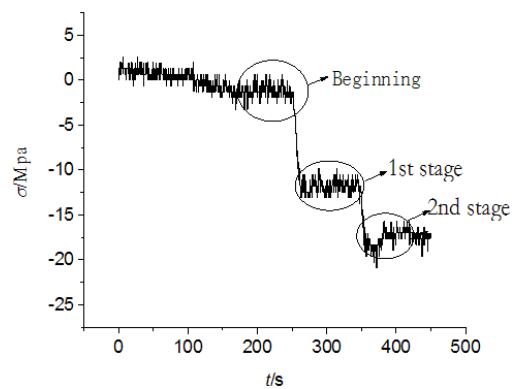


Fig. 37 Stress time-history of Z1-2 strut in second stage of cable tensioning

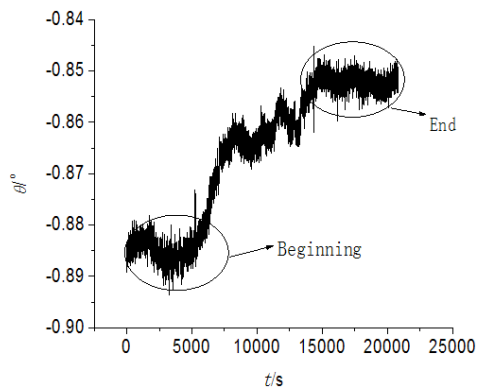


Fig. 38 Inclination time-history of 34# support in second stage of cable tensioning

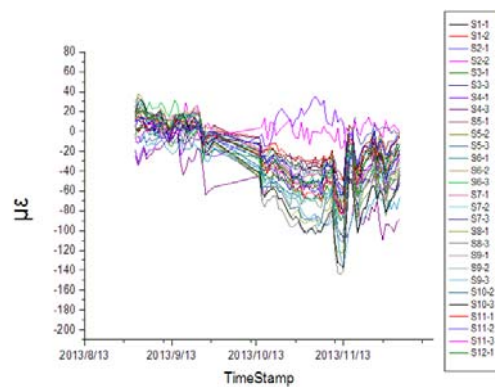
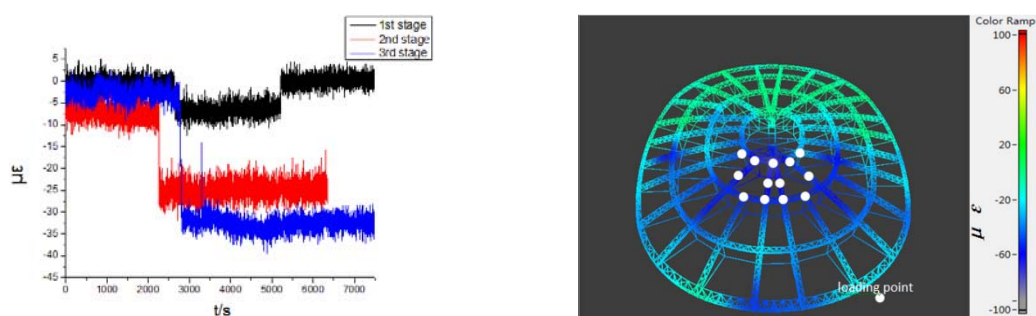


Fig. 39 Strain variation from August to December 2013

(b) Monitoring results of load tests on roof structure

On October 26th, 28th and 29th in 2013, there were load tests carried out on the roof structure divided into three stages. 20t, 35t and 60t were applied separately, Fig. 40(a). Using the 3D model displaying method, the distribution of strain on the whole roof structure is shown in Fig. 40(b), which indicates that the load application only effected local structure while the entire roof was still under safe condition.



(a) Time history of three different times load tests (b) 3D model display of the 3rd load test in real-time

Fig. 40 Monitoring results of load tests

5.2 Long-span bridges

The 1113 meter long Shenyang Boguan Bridge crosses the fast flowing Hun River in Shenyang in North Eastern China. The main span of bridge is 430 meters and the bridge is 32 meters wide. Shenyang Boguan Bridge is a “ribbon” style bridge with a 67 meter high arch; the parabola shaped structure is the most beautiful bridge to cross the Hun River. Fig. 41(a) shows the overview of the bridge. Shenyang Boguan Bridge is the first half-through 6-span “ribbon” style skew arch bridge in China. To ensure the safety during its construction and service, a complete set of SHM system was designed and installed on it. To perform the dynamic analysis and obtain the vibration characteristics of the bridge, a three dimensional finite element (FE) model was developed using the MIDAS-CIVIL software (MIDAS Information Technology Co., Ltd.), as shown in Fig. 41(b). It contains 6,597 Beam Elements, 174 Truss Elements, 1,518 Plate Element, and 6,365 nodes.

The SHM system architecture of the bridge is configured in four integrating modules comprising the sensor subsystem, data acquisition and transmission subsystem, data management subsystem, and condition assessment subsystem. 1) As shown in Fig. 42, the sensor subsystem is comprise five types of sensor: FBG strain sensors, FBG temperature sensors, accelerometers, anemometers, global positioning systems (GPS) revivers. These sensors collect the signals and deliver them to the PC-based data acquisition system through category 5 unshielded twisted-pair cables. 2) The data acquisition and transmission are the PC-based data acquisition units connected by fibre optic network. The data acquisition instruments, the si425 Optical Sensing Interrogator and NI PXI-1044 Chassis, both provide open data acquisition programs based on the LabVIEW platform. But these two data acquisition programs are mutually independent, so the signals of FBG sensors and electrical sensors can't be acquired synchronous. In order to integrate these two data

acquisition instruments, the data acquisition programs of NI PXI-1044 were embed into the si425 data acquisition software and developed a synchronous acquisition system for both optical and electrical sensors. By this synchronous acquisition system, the si425 Optical Sensing Interrogator and NI PXI-1044 Chassis could be simultaneously controlled and synchronous data acquisition of optical and electrical sensors is guaranteed. 3) The database manages the construction information, monitoring data and analysis results, which is the core part of SHM system and directly related to the efficiency the whole system. The relational and network database SQL Server 2000 is adopted as the central database of the SHM system. Correspondingly, Database Connectivity Toolkit (DCT), which encapsulates a series of senior function modules, is adopted in this system to access SQL Server 2000. 4) The condition assessment subsystem including four functions: security warning, model updating, damage identification, and safety assessment. Each subsystem is capable of stand-alone operation under normal and abnormal conditions irrespective of whether they are inter-connected together, i.e., failure of an individual module will have no detrimental effect on the remaining parts of the system.



Fig. 41 Shenyang Boguan Bridge and its FE model

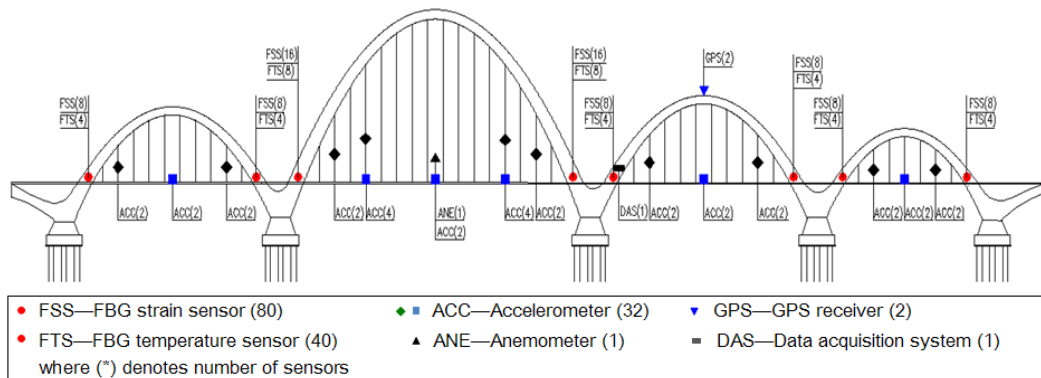


Fig. 42 Distribution of sensors in Shenyang Boguan Bridge

5.3 Large-scale offshore structures

(1) Monopile offshore platform

The FBG sensors were applied to the strain monitoring of oil production offshore platform No.CB271, located in the Bohai Sea of China. At the bottom of central pillar, three bare FBG sensors were placed as a strain rosette on the surface of pillar, and an FBG temperature sensor was placed close to those strain sensors for the temperature compensation. One year later, after this offshore platform had been built in the sea area of oil extraction, the FBG sensors installed in the bottom of central pillar were working well as expected, and did not show any significant reduction of sensing performance. However, the strain gauges placed near the FBG sensors failed to operate due to the detrimental corrosion of seawater (Fig. 43). In this aspect, the FBG sensors demonstrated distinct advantages for the long term health monitoring of ocean structures because of their reliability and durability.

(a) Ship collision

Supplying boat collision is one of the most critical accidents that can affect the structural safety of offshore platform and the integrity of fixed installation (Visser 2004). It is, therefore, significant to monitor the real-time strain variation of ship collision. A strain course induced by an impaction of ship with hundreds tons weight was recorded by the FBG sensors in July, 20, 2004. Fig. 43 exhibits a position of ship collision in this offshore platform, and Table 4 presents the maximum strain measured by the FBG strain sensors in three different directions. For the sensors located at the direct backside of the impaction, the maximum strains measured by FBG sensors are negative as shown in Fig. 44. The vertical strain measured by the 3# sensor is apparently greater than the horizontal one by the 1# sensor since the ship struck the pillar horizontally.

The directions of these FBG sensors placed by a strain rosette are $\alpha_1=0^\circ$, $\alpha_2=45^\circ$ and $\alpha_3=90^\circ$ respectively. From the principle of a standard textbook (Timoshenko and Gere 1972), it can be got: $\varepsilon_x=-19.1\mu\varepsilon$, $\varepsilon_y=-26.7\mu\varepsilon$, $\gamma_{xy}=-5.8\mu\varepsilon$. The maximum principal strain is $-27.7\mu\varepsilon$ and its direction is 251.3° . For this strain was in the range of platform linear elasticity, this boat collision did not bring any potential damage to the ocean platform.

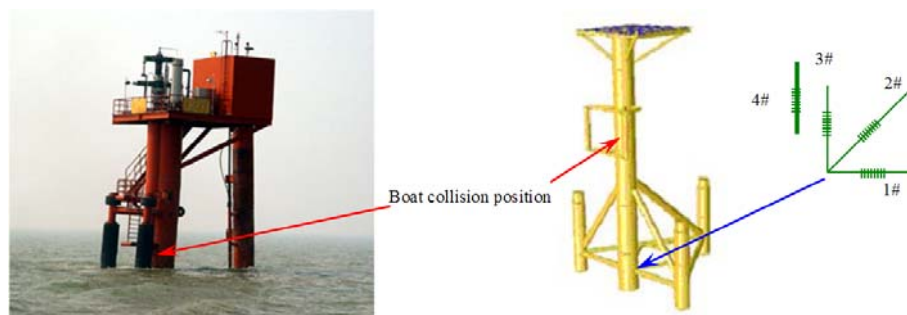


Fig. 43 Platform picture, model and sensors position

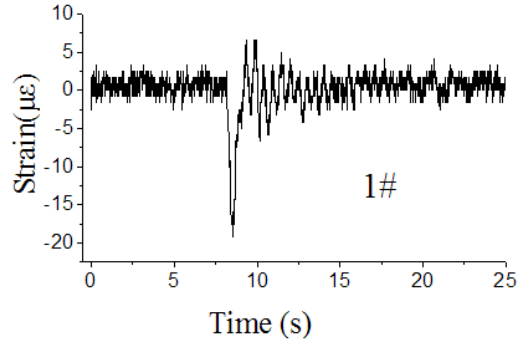


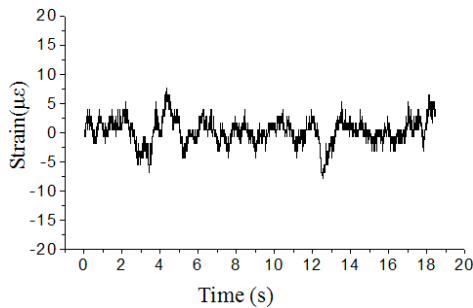
Fig. 44 Strain course induced by ship impaction by embedded FBG stain sensors

Table 4 Sensors specifications

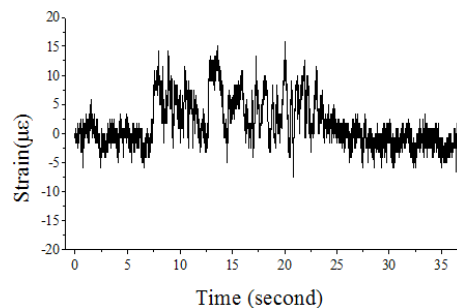
Name	Position	Wavelength (nm)	Maximum Strain (µε)
1#	0°	1530nm	6.7 -19.1
2#	45°	1540nm	9.1 -25.8
3#	90°	1550nm	9.2 -26.7

(b) Ocean wave loads

Ocean wave is another critical factor that can influence the structural health of an ocean platform. The strain variation of offshore platform in the Bohai Sea induced by normal ocean wave loads was monitored by these FBG strain sensors as shown in Fig. 45(a). In the course of strain measurement, these FBG sensors monitored an abnormal process of ocean current impaction, which lasted about 20 seconds as shown in Fig. 45(b). The intensity of this ocean current was apparently greater than the normal ocean wave presented ahead. Comparing the maximum strain of ship collision with the ocean wave, the intensity of later was not much less than the former. The influence of ocean wave impaction cannot be negligible during the period of oil ocean platform operation.



(a) Normal Ocean wave



(b) Abnormal ocean wave

Fig. 45 Strain course induced by ship impaction by embedded FBG stain sensors

(2) Offshore jacket platform

An oil production offshore jacket platform in the Bohai Sea of China was instrumented with 40 FBG sensors and monitored for the piles loading under the condition of platform construction and operation as it is shown in Fig. 46. The aim of this study was to provide a realistic assessment of integrity of the foundation piles for future use. The stress loads in the pile heads were transferred from the total weight of the upper structure of platform through the six piles. The weight variation of the upper structure of platform would cause the elastic deformation of six upright piles and be monitored in real-time by the FBG strain sensors installed in the surface of piles. To eliminate the stress bias influenced by the buckling stress and the eccentricity of piles, every 4 FBG strain sensors were mounted on each pile evenly along the pile hoop as it is shown in Fig. 46. In addition, one FBG temperature sensor was installed in each pile to compensate the stress shift of temperature variation.

After the sensors and the demodulation system installation, a calibration test for the system commissioning was carried out to investigate the effectiveness of SHM system. A series of lifting tasks were executed in one and a half hours by the run-operator of platform to convey the equipment of drilling from the transportation ship to the platform. The whole process of lifting tasks was monitored in real-time by the SHM system and the loading result agreed well with the record provided by the crane as it is shown in Fig. 47. It can be seen that there were seven wave crests in the Fig. 48 which happened in the pile B3 and apparently induced by the cargo lifting and discharging process of crane. The Fig. 49 presents the variation of total weight of upper structure of platform in two months monitored by the SHM system. It can be drawn that this offshore platform was under safe condition for that the maximum load of the upper structure platform and the pile heads were separately about 73% and 40% to 70% of the total weight which was much less than the alert load that is 85% of the total weight.

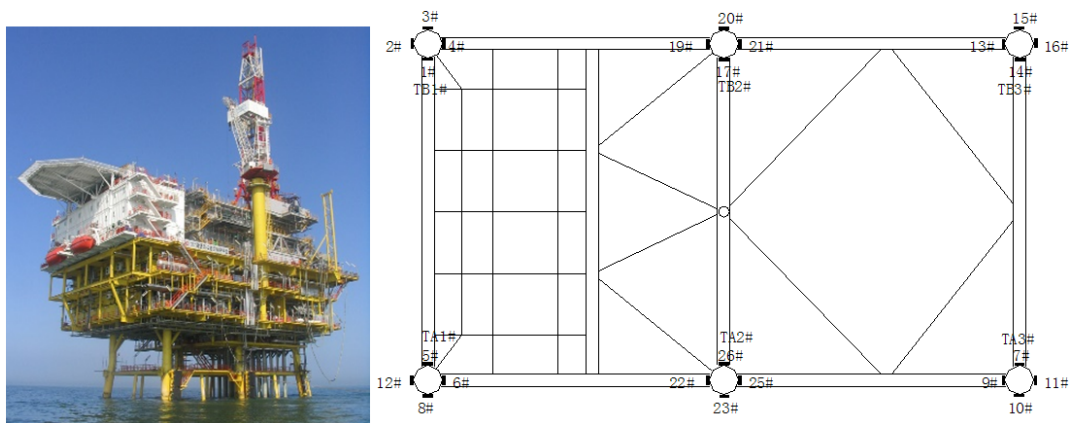


Fig. 46 Offshore platform and position of FBG sensors on piles of platform

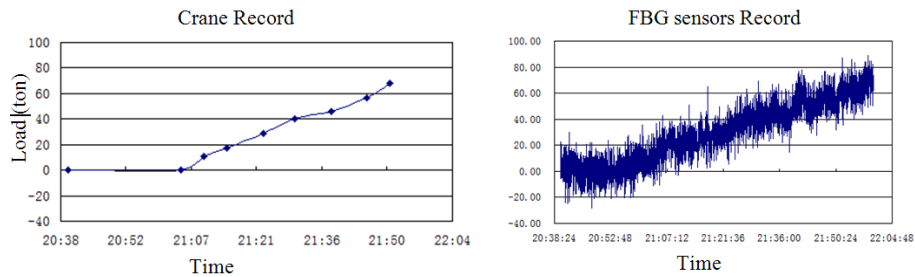


Fig. 47 Process of lifting tasks and variation of loads of upper structure

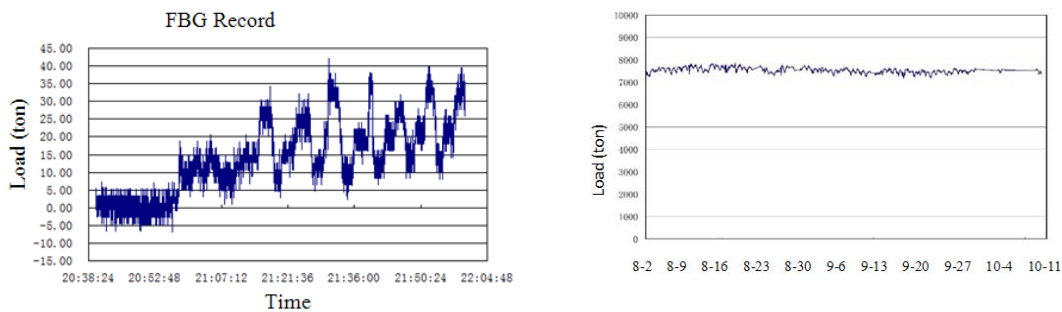


Fig. 48 Variation of loads of pile B3

Fig. 49 Variation of total weight of the upper structure

In this project, the SHM system based in the FBG sensors exhibits its unique advantages in the field of offshore engineering ranging from its long-term durability, good reliability, immunity to EMI and well flexibility of installation. Some further work should still be conducted to overcome the shortcomings of FBG sensors exposed in this project such as the strain bias induced by the effect of temperature variation, anticorrosion measures and small optical signal identification.

6. Conclusions

The SHM is a topic that has gained a significant high attention in the last decades. This paper explores the recent technology and methodology developments in the field of SHM and their application to large-scale infrastructures carried out by the faculty members at Dalian University of Technology. Along with a huge volume of literature published relating to the SHM around the world and our research work, the existing problems and promising research efforts in this field appears to be reached some consensus, which are as follows:

- Development of reliable SHM system including the distributed and embedded sensing (the MEMS & nano-engineered sensors, Wireless sensors, Ultrasonic/guided wave sensors, Bio-inspired sensors and actuators, etc.), communication system (the robust low-cost wireless systems, economic land links system, efficient data compression and preprocessing techniques, optimal network layout method, etc.), data management and storage equipment (the elaborate database system, effective security measures, etc.).

- Development of efficient data analysis methods for vast amounts of monitoring data including the data-driven structural condition evaluation based on wired or wireless system, nature-inspired intelligent computational methods for the data mining, damage detection and system identification by use of the real-world monitoring data, reliability-based structural condition/safety assessment with uncertainties, novel analytical models for structural feature extraction, etc.
- Development of standardization of SHM principles and best-practices including rational roadmap towards a globally harmonized approach to the SHM code and standard development, trends in the research community aiming towards field deployment of SHM to operational structures, learning from other sectors outside of civil and hydraulic engineering, consideration for the SHM to be incorporated at the design stage, etc.

Acknowledgements

This research work was jointly supported by the National Natural Science Foundation of China (Grant No. 51121005, 51222806, 51327003), the Fok Ying Tong Education Foundation (141072), and the Specialized Research Fund for the Doctoral Program of Higher Education (Grant No. 20130041110031).

References

- Aktan, A.E. and Catbas, F.N. (2003), *Development of a model health monitoring guide for major bridges*, Federal Highway Administration Research and Development for CONTRACT/ORDER NO. DTFH61-01-P-00347.
- Ansari, F. and Libo, Y. (1998), "Mechanics of bond and interface shear transfer in optical fiber sensors", *J. Eng. Mech.-ASCE*, **124**(4), 385-394.
- Balageas, D., Fritzen, C.P. and Güemes, A. (2006), *Structural health monitoring*, ISTE, London, UK.
- Baldwin, C., Salter, T., Niemczuk, J., Chen, P. and Kiddy, J. (2002), "Structural monitoring of composite marine piles using multiplexed fiber Bragg grating sensors: In-field applications", *Smart Structures and Materials 2002: Smart Systems for Bridges, Structures, and Highways*, (Eds. S.C. Liu and D.J. Pines), *Proceedings of the SPIE*, San Diego, USA.
- Bai, H.F., Yi, T.H., Li, H.N. and Ren, L. (2012), "Multisensors on-site monitoring and characteristic analysis of UHV transmission tower", *Int. J. Distrib. Sens. N.*, Article ID 545148, 1-10.
- Bergmeister, K. (2002), *Monitoring and safety evaluation of existing concrete structures: state-of-the-art report*, Fib Task Group 5.1.
- Betz, D.C., Thursby, G., Culshaw, B. and Staszewski, W.J. (2003), "Acousto-ultrasonic sensing using fiber Bragg gratings", *Smart Mater. Struct.*, **12**(1), 122-128.
- Bhalla, S. and Soh, C.K. (2003), "Structural impedance based damage diagnosis by piezo-transducers", *Earthq. Eng. Struct. D.*, **32**(12), 1897-1916.
- Brownjohn, J.M. (2007), "Structural health monitoring of civil infrastructure", *Philos. T. R. Soc. A.*, **365**(1851), 589-622.
- Brownjohn, J.M.W. and Moyo, P. (2001), "Monitoring of Singapore-Malaysia second link during construction", *Proceedings of the 2nd International Conference on Experimental Mechanics*, Singapore, June.
- Carne, T.G. and Dohrmann, C.R. (1995), "A modal test design strategy for model correlation", *Proceedings of the 13th International Modal Analysis Conference*, Nashville, USA, February.
- Chen, S., Chen, Z. and Wang, W. (2010), "Multi-scale detection techniques for local scour monitoring in

- river bed: case study at Sutong Bridge”, *Proceeding of the Earth and Space 2010: Engineering, Science, Construction*, Hawaii, USA, March.
- Cheung, M.S., Tadros, G.S., Brown, T., Dilger, W.H., Ghali, A. and Lau, D.T. (1997), “Field monitoring and research on performance of the Confederation Bridge”, *Can. J. Civil. Eng.*, **24**(6), 951-962.
- Cigada, A., Moschioni, G., Vanali, M. and Caprioli, A. (2010), “The measurement network of the San Siro Meazza stadium in Milan: origin and implementation of a new data acquisition strategy for structural health monitoring”, *Exp. Techniques*, **34**(1), 70-81.
- Cox, H. (1952), “The elasticity and strength of paper and other fibrous materials”, *Br. J. Appl. Phys. s*, **3**(3), 72-79.
- Cullington, D.W., MacNeil, D., Paulson, P. and Elliot, J. (1999), “Continuous acoustic monitoring of grouted post-tensioned concrete bridges”, *Proceedings of the 8th International Structural Faults and Repair Conference*, London, UK, June.
- Design code (2012), *Design standard for structural health monitoring systems (CECS 333: 2012)*, Standard for China Association for Engineering Construction Standardization, Beijing, China.
- Dijk, R.V. and Boom, Henk. V.D. (2007), “Full scale monitoring Marco Polo tension leg platform”, *Proceedings of the 26th International Conference on Offshore Mechanics and Arctic Engineering*, CA, USA, June.
- Farrar, C.R. and Worden, K. (2013). *Structural health monitoring - a machine learning perspective*, John Wiley & Sons Ltd, Chichester, UK.
- Friebele, E.J., Askins, C.G., Bosse, A.B., Kersey, A.D., Patrick, H.J., Pogue, W.R., Putnam, M.A., Simon, W. R., Tasker, F.A., Vincent, W.S. and Vohra, S.T. (1999), “Optical fiber sensors for spacecraft applications”, *Smart Mater. Struct.*, **8**(6), 813-838.
- Galiotis, C., Young, R., Yeung, P. and Batchelder, D. (1984), “Study of model polydiacetylene/epoxy composites. Part 1- the axial strain in the fibre”, *J. Mater. Sci.*, **19**(11), 3640-3648.
- Hejll, A. (2007), *Civil structural health monitoring -strategies, methods and applications*, Ph.D. Dissertation, Luleå University of Technology, Luleå.
- Henrik, L.J. and Denmark, S.E. (2002), “Analyzing Europe’s largest suspension bridge”, *Proceedings of the FIG XXII International Congress*, Washington, USA, April.
- Hernandez-Garcia M.R., Masri S.F., Ghanem R., Figueiredo E. and Farrar C.R. (2010), “An experimental investigation of change detection in uncertain chain-like systems”, *J. Sound Vib.*, **329**(12), 2395-2409.
- Housner, G.W., Bergman, L.A., Caughey, T.K., Chassiakos, A.G., Claus, R.O., Masri, S.F., Soong, T.T., Spencer, B. F. and Yao, J.T.P. (1997), “Structural control: past, present, and future”, *J. Struct. Eng.- ASCE*, **123**(9), 897-971.
- ISO (2002), *Mechanical vibrations evaluation of results from dynamic tests and investigations of bridges*, ISO 18649.
- Jahani, K. and Nobari, A. (2008), “Identification of dynamic (Youngs and shear) moduli of a structural adhesive using modal based direct model updating method”, *Exp. Mech.*, **48**(5), 599-611.
- James G.H., Carne T.G. and Lauffer J.P. (1993), *The natural excitation technique (NExT) for modal parameter extraction from operating wind turbines*, Sandia National Labs Report, Albuquerque, NM.
- James G.H., Carne T.G. and Mayes R.L. (1996), “Modal parameter extraction from large operating structures using ambient excitation”, *Proceedings of the 14th International Modal Analysis Conference*, Orlando, Florida, USA, February.
- Jiao, L. and Li, H.N. (2006), “A data fusion method based on improved consensus algorithm”, *J. Disaster Prevention Mitigation Eng.*, **26**(2), 170-174.
- Kammer, D.C. (1991), “Sensor placement for on-orbit modal identification and correlation of large space structures”, *J. Guid. Control Dynam.*, **14**(2), 251-259.
- Kammer, D.C. and Tinker, M.L. (2004), “Optimal placement of tri-axial accelerometers for modal vibration tests”, *Mech. Syst. Signal Pr.*, **18**(1), 29-41.
- Kashima, S., Yanaka, Y. and Suzuki, S. (2001), “Monitoring the Akashi Kaikyo bridge: first experiences”, *Struct. Eng. Int.*, **11**(2), 120-123.
- Kijewski-Correa, T., Kareem, A. and Kochly, M. (2006), “Experimental verification and full-scale

- deployment of Global Positioning Systems to monitor the dynamic response of tall buildings”, *J. Struct. Eng.- ASCE*, **132**(8), 1242-1253.
- Ko, J.M. and Ni, Y.Q. (2005), “Technology developments in structural health monitoring of large-scale bridges”, *Eng. Struct.*, **27**(12), 1715-1725.
- Lai, T., Yi, T.H. and Li, H.N. (2010), “Multi-rate data fusion for dynamic response data using adaptive kalman filtering”, *Proceedings of the 9th International Conference on Civil and Environmental Engineering*, Dalian, China, November.
- Lee E.T. and Eun H.C. (2008), “Damage detection of damage beam by constrained displacement curvature”, *J. Mech. Sci. Technol.*, **22**(6), 1111-1120.
- Liang, C., Sun, F.P. and Rogers, C.A. (1994), “Coupled electro-mechanical analysis of adaptive material systems: determination of the actuator power consumption and system energy transfer”, *J. Intel. Mat. Syst. Str.*, **5**(1), 12-20.
- Liang, Y.B., Li, D.S. and Li, H.N. (2014), “Online damage detection based on the combination of successive displacement curvature under the influence of environmental temperature”, Submitted to *J. Dalian Univ. Tech.*.
- Li, D.S., Li, H.N. and Fritzen, C.P. (2007), “The connection between Effective independence and modal kinetic energy methods for sensor placement”, *J. Sound Vib.*, **305**(4-5), 945-955.
- Li, D.S., Li, H.N. and Fritzen, C.P. (2009), “A note on fast computation of effective independence through QR downdating for sensor placement”, *Mech. Syst. Signal Pr.*, **23**(4), 1160-1168.
- Li, D.S., Li, H.N. and Fritzen, C.P. (2012), “Load dependent sensor placement method: Theory and experimental validation”, *Mech. Syst. Signal Pr.*, **31**(1), 217-227.
- Li, D.S., Li, H.N., Ren, L. and Song, G. (2006), “Strain transferring analysis of fiber Bragg grating sensors”, *Opt. Eng.*, **45**(2), 4402.
- Li, H.N., Gao, D.W. And Yi, T.H. (2008), “Advances in structural health monitoring system in civil engineering”, *Adv. Mech.*, **38**(2), 151-166.
- Li, H.N., He, X.Y. and Yi, T.H. (2009a), “Multi-component seismic response analysis of offshore platform by wavelet energy principle”, *Coast. Eng.*, **56**(8), 810-830.
- Li, H.N. and Li, D.S. (2002), “Safety assessment, health monitoring and damage diagnosis for structures in civil engineering”, *Earthq. Eng. Eng. Vib.*, **22**(3), 82-90.
- Li, H.N., Li, D.S. and Song, G.B. (2004), “Recent applications of fiber optic sensors to health monitoring in civil engineering”, *Eng. Struct.*, **26**(11), 1647-1657.
- Li, H.N., Yi, T.H., Gu, M. and Huo, L.S. (2009b), “Evaluation of earthquake-induced structural damages by wavelet transform”, *Prog. Nat. Sci.*, **19**(4), 461-470.
- Li, H.N., Yi, T.H., Yi, X.D. and Wang, G.X. (2007), “Measurement and analysis of wind-induced response of tall building based on GPS technology”, *Adv. Struct. Eng.*, **10**(1), 83-93.
- Li, H.N., Zhou, G.D., Ren, L. and Li, D.S. (2007), “Strain transfer analysis of embedded fiber Bragg grating sensor under nonaxial stress”, *Opt. Eng.*, **46**(5), 054402.
- LI, H.N., Zhou, G.D., Ren, L. and Li, D.S. (2009), “Strain transfer coefficient analyses for embedded fiber Bragg grating sensors in different host materials”, *J. Eng. Mech.- ASCE*, **135**(12), 1343-1353.
- Limongelli, M.P. (2003), “Optimal location of sensors for reconstruction of seismic responses through spline function interpolation”, *Earthq. Eng. Struct. D.*, **32**(7), 1055-1074.
- Li, Q., Li, G., Wang, G., Ansari, F. and Liu, Q. (2002), “Elasto-plastic bonding of embedded optical fiber sensors in concrete”, *J. Eng. Mech.- ASCE*, **128**(4), 471-478.
- Li, X., Huo, L.S. and Li, H.N. (2012), “Beat phenomenon analysis of concrete beam with piezoelectric sensors”, *Int. J. Distrib. Sens. N.*, **2012**(2012), Article ID 296124.
- Magne, S., Boussoir, J., Rougeault, S., Marty-Dewynter, V., Ferdinand, P. and Bureau, L. (2003), “Health monitoring of the Saint-Jean bridge of Bordeaux, France using fiber Bragg grating extensometers”, *Proceedings of the SPIE 5050, Smart Structures and Materials 2003: Smart Sensor Technology and Measurement Systems*, CA, USA, July.
- Masri S., Bekey G., Sassi H. and Caughey T. (1982), “Non-parametric identification of a class of nonlinear

- multidegree dynamic systems”, *Earthq. Eng. Struct. D.*, **10**(1), 1-30.
- Mohamad, H., Bennett, P., Soga, K., Mair, R., Lim, C., Knight-Hassell, C. and Ow, C. (2007), “Monitoring Tunnel Deformation induced by close-proximity bored tunneling using distributed optical fiber strain measurements”. *Proceeding of the 7th International Symposium on Field Measurements in Geomechanics*, Boston, USA, September.
- Mufti, A.A. (2001), *Guidelines for structural health monitoring*, ISIS Canada.
- Mufti, A.A. (2002), “Structural health monitoring of innovative Canadian civil engineering”, *Struct. Health. Monit.*, **1**(1), 89-103.
- Nayeri R.D., Masri S.F., Ghanem R.G. and Nigbor R.L. (2008), “A novel approach for the structural identification and monitoring of a full-scale 17-story building based on ambient vibration measurements”, *Smart Mater. Struct.*, **17**(2), 025006.
- Ni, Y.Q., Xia, Y., Liao, W.Y. and Ko, J.M. (2009), “Technology innovation in developing the structural health monitoring system for Guangzhou New TV Tower”, *Struct. Control Health Monit.*, **16**(1), 73-98.
- Pak, Y. (1992), “Longitudinal shear transfer in fiber optic sensors”, *Smart Mater. Struct.*, **1**(1), 57-62.
- Papadimitriou, C. (2004), “Optimal sensor placement methodology for parametric identification of structural systems”, *J. Sound Vib.*, **278**(4-5), 923-947.
- Papadopoulos, M. and Garcia, E. (1998), “Sensor placement methodologies for dynamic testing”, *AIAA J.*, **36**(2), 256-263.
- Peeters, B. and Roeck, G.D. (2001), “One-year monitoring of the Z24-Bridge: environmental effects versus damage events”, *Earthq. Eng. Struct. D.*, **30**(2), 149-171.
- Penny, J.E.T., Friswell, M.I. and Garvey, S.D. (1994), “Automatic choice of measurement locations for dynamic testing”, *AIAA J.*, **32**(2), 407-414.
- Ran, L., Yi, T.H., Ye, X.W. and Dong, X.B. (2012), “Long-term deformation monitoring of metro-tunnel airshaft excavation during construction stage”, *Int. J. Distrib. Sens. N.*, Article ID 972893, 1-11.
- Ren, L., Chen, J.Y. and Li, H.N. (2009), “Design and application of a fiber Bragg grating strain sensor with enhanced sensitivity in the small-scale dam model”, *Smart Mater. Struct.*, **18**(3), 11-15.
- Ren, L., Li, H.N., Li, D.S. and Zhou, J. (2006), “Health monitoring system for offshore platform with fiber Bragg grating sensors”, *Opt. Eng.*, **45**(8), Article ID 084401, 1-9.
- Ritdumrongkul, S. and Fujino, Y. (2007), “Identification of the location and size of cracks in beams by a piezoceramic actuator-sensor”, *Struct. Control Health Monit.*, **14**(6), 931-943.
- Rucker, W., Hille, F. and Rohrmann, R. (2006), *Guideline for structural health monitoring*, SAMCO F08b.
- Schenewerk, M.S., Harris, R.S. and Stowell, J. (2006), “Structural health monitoring using GPS: observing the Sunshine Skyway Bridge”, *Bridges*, **4**, 18-25.
- Shang, H.S., Yi, T.H. and Yang, L.S. (2012), “Experimental study on the compressive strength of big mobility concrete with nondestructive testing method”, *Adv. Mater. Sci. Eng.*, Article ID 345214, 1-6.
- Song, G.B., Gu, H.C. and Mo, Y.L. (2008), “Smart aggregates: multi-functional sensors for concrete structures - a tutorial and a review”, *Smart Mater. Struct.*, **17**(3), 1-17.
- Stubbs, N. and Park, S. (1996), “Optimal sensor placement for mode shapes via Shannon's sampling theorem”, *Microcomput. Civ. Eng.*, **11**(6), 411-419.
- Tawie, R. and Lee, H.K. (2010), “Monitoring the strength development in concrete by EMI sensing technique”, *Constr. Build Mater.*, **24**(9), 1746-1753.
- Timoshenko, S. (1956), *Strength of material, part ii, elementary theory and problems*, D Van Nostrand Co., Inc. New York, USA.
- Trendafilova, I., Heylen, W. and Brussel, H. Van. (2001), “Measurement point selection in damage detection using the mutual information concept”, *Smart Mater. Struct.*, **10**(3), 528-533.
- Udd, E. (1995), *Fiber optic smart structures*, Wiley-Interscience, New York, NY, USA.
- Visser, W. (2004), *Ship collision and capacity of brace members of fixed steel offshore platforms*, HSE books, research report 220, 1-10.
- Wan, K.T., Leung, C.K.Y. and Olson, N.G. (2008), “Investigation of the strain transfer for surface-attached optical fiber strain sensors”, *Smart Mater. Struct.*, **17**(3), Article ID 035037.
- Wenzel, H. (2009), *Health monitoring of bridges*, John Wiley & Sons, New York, USA.

- Wong, K.Y. (2004), "Instrumentation and health monitoring of cable-supported bridges", *Struct. Control Health Monit.*, **11**(2), 91-124.
- Ye, X.W., Ran, L., Yi, T.H. and Dong, X.B. (2012), "Intelligent risk assessment for dewatering of metro-tunnel deep excavations", *Math. Probl. Eng.*, Article ID 618979, 1-13.
- Yi, T.H. and Li, H.N. (2006), "High accuracy GPS deformation monitoring via errors cancelling by ANC and wavelet analysis", *Proceedings of the 10th ASCE Aerospace Division Conference on Engineering, Construction and Operations in Challenging Environments*, Houston, TX, USA, March.
- Yi, T.H. and Li, H.N. (2009), *Structural health monitoring based on GPS technology*, China Architecture & Building Press, Beijing, China.
- Yi, T.H., Li, H.N. and Gu, M. (2010a), "Recent research and applications of GPS based technology for bridge health monitoring", *Sci. China Technol. Sc.*, **53**(10), 2597-2610.
- Yi, T.H., Li, H.N. and Gu, M. (2010b), "Full-scale measurement of dynamic response of a suspension bridge subjected to environmental loads using GPS technology", *Sci. China Technol. Sc.*, **53**(2), 469-479.
- Yi, T.H., Li, H.N. and Gu, M. (2011a), "A new method for optimal selection of sensor location on a high-rise building using simplified finite element model", *Struct. Eng. Mech.*, **37**(6), 671-684.
- Yi, T.H., Li, H.N. and Gu, M. (2011b), "Characterization and extraction of global positioning system multipath signals using improved particle filtering algorithm", *Meas. Sci. Technol.*, **22**, Article ID 075101: 1-11.
- Yi, T.H., Li, H.N. and Gu, M. (2011c), "Optimal sensor placement for health monitoring of high-rise structure based on genetic algorithm", *Math. Probl. Eng.*, Article ID 395101, 1-11.
- Yi, T.H., Li, H.N. and Gu, M. (2011d), "Optimal sensor placement for structural health monitoring based on multiple optimization strategies", *Struct. Des. Tall Spec.*, **20**(7), 881-900.
- Yi, T.H. and Li, H.N. (2012a), "Methodology developments in sensor placement for health monitoring of civil infrastructures", *Int. J. Distrib. Sens. N.*, Article ID 612726, 1-11.
- Yi, T.H., Li, H.N. and Gu, M. (2012b), "Effect of different construction materials on propagation of GPS monitoring signals", *Measurement*, **45**(5), 1126-1139.
- Yi, T.H., Li, H.N. and Gu, M. (2012c), "Sensor placement for structural health monitoring of Canton Tower", *Smart Struct. Syst.*, **10**(4-5), 313-329.
- Yi, T.H., Li, H.N. and Zhang, X.D. (2012d), "A modified monkey algorithm for optimal sensor placement in structural health monitoring", *Smart Mater. Struct.*, **21**(10), Article ID 05033, 1-9.
- Yi, T.H., Li, H.N. and Zhang, X.D. (2012e), "Sensor placement on Canton Tower for health monitoring using asynchronous-climb monkey algorithm", *Smart Mater. Struct.*, **21**(12), 1-12.
- Yi, T.H., Li, H.N. and Zhao, X.Y. (2012f), "Noise smoothing for structural vibration test signals using an improved wavelet thresholding technique", *Sensors*, **12**(8), 11205-11220.
- Yi, T.H., Li, H.N. and Gu, M. (2013a), "Experimental assessment of high-rate GPS receivers for deformation monitoring of bridge", *Measurement*, **46**(1), 420-432.
- Yi, T.H., Li, H.N. and Gu, M. (2013b), "Recent research and applications of GPS-based monitoring technology for high-rise structures", *Struct. Control Health Monit.*, **20**(5), 649-670.
- Yi, T.H., Li, H.N. and Gu, M. (2013c), "Wavelet based multi-step filtering method for bridge health monitoring using GPS and accelerometer", *Smart Struct. Syst.*, **11**(4), 331-348.
- Yi, T.H., Li, H.N. and Sun, H.M. (2013d), "Multi-stage structural damage diagnosis method based on "energy-damage" theory", *Smart Struct. Syst.*, **12**(3-4), 345-361.
- Yi, T.H., Li, H.N. and Wang, X. (2013e), "Multi-dimensional sensor placement optimization for Canton Tower focusing on application demands", *Smart Struct. Syst.*, **12**(3-4), 235-250.
- Yoo, K. and Park, H. (1996), "Accurate downdating of a modified Gram-Schmidt QR decomposition", *BIT*, **36**(1), 166-181.
- Zhan, C., Li, D.S. and Li, H.N. (2013), "A local damage detection approach based on restoring force method", Submitted to *J. Sound Vib.*
- Zhao, R.Q. and Tang, W.S. (2008), "Monkey algorithm for global numerical optimization", *J. Uncer. Syst.*, **2**(3), 165-176.
- Zhao, X.Y. (2008), *Structure health monitoring and damage detection based on piezoelectric ceramic*

- transducers*, Ph.D. Dissertation, Dalian University of Technology, Dalian, China.
- Zhao, X.Y. and Li, H.N. (2008a), "Concrete structure monitoring based on built-in piezoelectric ceramic transducers", *Proceedings of the SPIE: Smart Structures and Materials Symposium*, San Jose, USA, March.
- Zhao, X.Y. and Li, H.N. (2008b), *Parameters identification of concrete structure based on built-in PZT sensors*, Earth & Space, Longbeach, USA, March.
- Zhou, G.D. and Yi, T.H. (2013a), "Recent developments on wireless sensor networks technology for bridge health monitoring", *Math. Probl. Eng.*, Article ID 947867, 1-33.
- Zhou, G.D. and Yi, T.H. (2013b), "The node arrangement methodology of wireless sensor networks for long-span bridge health monitoring", *Int. J. Distrib. Sens. N.*, Article ID 865324, 1-8.
- Zhou, G.D. and Yi, T.H. (2013c), "The nonuniform node configuration of wireless sensor networks for long-span bridge health monitoring", *Int. J. Distrib. Sens. N.*, Article ID 797650, 1-9.
- Zhou, G.D. and Yi, T.H. (2013d), "Thermal load in large-scale bridges: a state-of-the-art review", *Int. J. Distrib. Sens. N.*, Article ID 217983, 1-17.
- Zhou, J., Zhou, Z. and Zhang, D. (2010), "Study on strain transfer characteristics of fiber Bragg grating sensors", *J. Intel. Mat. Syst. Struct.*, **21**(11), 1117-1122.